Mantle flow, volatiles, slab-surface temperatures and melting dynamics in the north Tonga arc–Lau back-arc basin

John Caulfield,[1] Simon Turner,[1] Richard Arculus,[2] Chris Dale,[3] Frances Jenner,[4] Julian Pearce,[5] Colin Macpherson,[3] and Heather Handley[1]

Received 13 June 2012; revised 2 October 2012; accepted 3 October 2012; published 21 November 2012.

[1] The Fonualei Spreading Center affords an excellent opportunity to evaluate geochemical changes with increasing depth to the slab in the Lau back-arc basin. We present H_2O and CO_2 concentrations and Sr, Nd, Pb, Hf and U-Th-Ra isotope data for selected glasses as well as new Hf isotope data from boninites and seamounts to the north of the Tonga arc. The Pb and Hf isotope data are used to show that mantle flow is oriented to the southwest and that the tear in the northern end of the slab may not extend east as far as the boninite locality. Along the Fonualei Spreading Center, key geochemical parameters change smoothly with increasing distance from the arc front and increasing slab surface temperatures. The latter may range from 720 to 866°C, based on decreasing H_2O/Ce ratios. Consistent with experimental data, the geochemical trends are interpreted to reflect changes in the amount and composition of wet pelite melts or super-critical fluids and aqueous fluids derived from the slab. With one exception, all of the lavas preserve both ^{238}U excesses and ^{226}Ra excesses. We suggest that lavas from the Fonualei Spreading Center and Valu Fa Ridge are dominated by fluid-fluxed melting whereas those from the East and Central Lau Spreading Centers, where slab surface temperatures exceed ~850–900°C, are largely derived through decompression. A similar observation is found for the Manus and East Scotia back-arc basins and may reflect the expiry of a key phase such as lawsonite in the subducted basaltic crust.

Citation: Caulfield, J., S. Turner, R. Arculus, C. Dale, F. Jenner, J. Pearce, C. Macpherson, and H. Handley (2012), Mantle flow, volatiles, slab-surface temperatures and melting dynamics in the north Tonga arc–Lau back-arc basin, *J. Geophys. Res.*, *117*, B11209, doi:10.1029/2012JB009526.

1. Introduction

[2] Back-arc basin basalts demonstrably have a more complex origin than their mid-ocean ridge counterparts and several recent studies have employed both trace elements and radiogenic isotopes in conjunction with U-series isotopes to investigate changes in source composition and the relative roles of fluid-fluxed and decompression melting [e.g., *Peate et al.*, 2001; *Fretzdorff et al.*, 2003; *Beier et al.*, 2010]. Such data provide an important complement to the application of major elements to constrain the conditions under which partial melting took place [e.g., *Taylor and Martinez*, 2003; *Kelley et al.*, 2006; *Langmuir et al.*, 2006; *Bézos et al.*, 2009]. The Lau Basin is a rapidly opening back-arc basin situated behind the Tonga arc (Figure 1) and both major element and seismic inversions indicate a mantle potential temperature around 1450°C, intermediate between the very hot Manus Basin and the cooler Mariana Trough [*Wiens et al.*, 2006; *Kelley et al.*, 2006]. Of the back-arc basins that have been studied in detail, the Lau Basin has been of particular interest because of the presence of a number of spreading centers (see Figure 1) that are oriented obliquely to the arc front [*Zellmer and Taylor*, 2001]. These have been exploited to delineate changes in lava composition with increasing distance from the arc, with particular focus on the Valu Fa Ridge and Central and Eastern Lau Spreading Centers [e.g., *Hergt and Hawkesworth*, 1994; *Pearce et al.*, 1995; *Peate et al.*, 2001].

[3] Recently, *Keller et al.* [2008] have highlighted the opportunity for samples dredged from the less well-studied, Fonualei Spreading Center to augment these earlier studies. Accordingly, we present new volatile measurements, radiogenic isotope and U-series data from selected samples from this region in order to further expand our understanding of this increasingly well-characterized island arc – back-arc system. These are augmented with new Hf isotope analyses of boninites and seamounts to the north of Tonga. The data

[1]GEMOC, Department of Earth and Planetary Sciences, Macquarie University, Sydney, New South Wales, Australia.
[2]Research School of Earth Sciences, Australian National University, Canberra, ACT, Australia.
[3]Department of Earth Sciences, University of Durham, Durham, UK.
[4]Department of Terrestrial Magnetism, Carnegie Institution of Washington, Washington, D. C., USA.
[5]School of Earth and Ocean Sciences, Cardiff University, Wales, UK.

Corresponding author: S. Turner, GEMOC, Department of Earth and Planetary Sciences, Macquarie University, Sydney, NSW 2109, Australia. (simon.turner@mq.edu.au)

0148-0227/12/2012JB009526

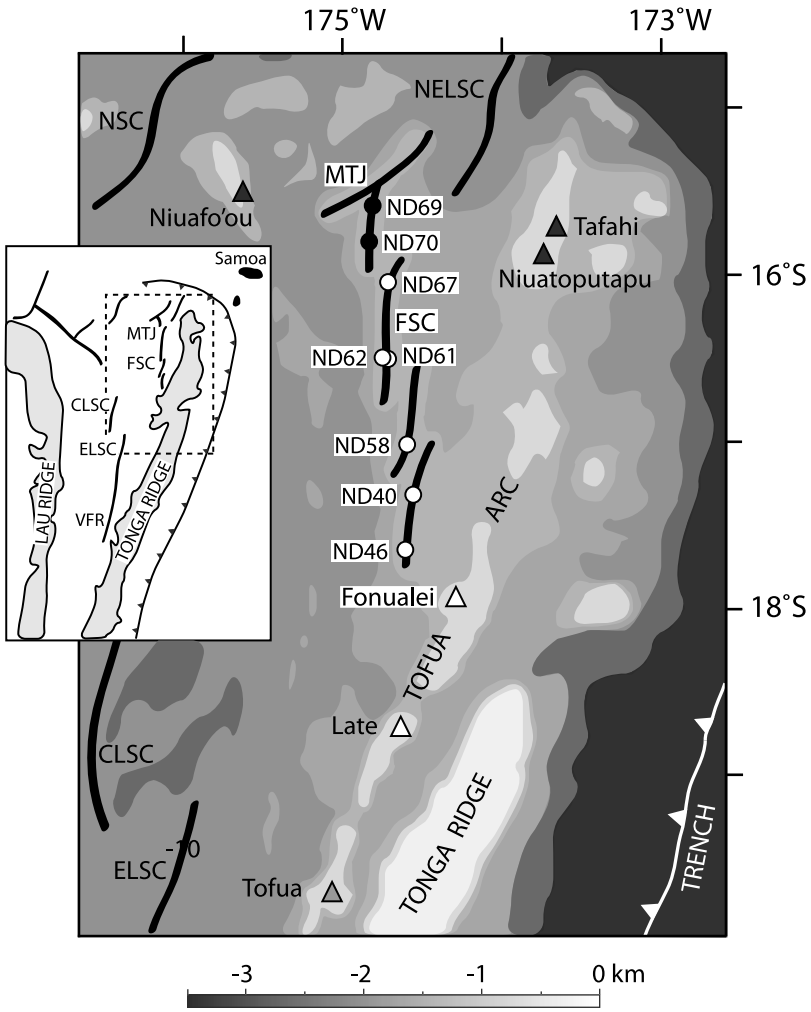

Figure 1. Map of the Fonualei Spreading Center showing the locations of samples analyzed in this study: Fonualei Spreading Center (FSC, unfilled circles); Mangatolu Triple Junction (MTJ, filled circles). Also included are the locations of Tofua arc islands: Tofua (shaded triangle); the FSC proximal islands of Late and Fonualei (unfilled triangles); and the northern islands of Niuatoputapu and Tafahi (filled triangles). Inset shows the location within the Tonga arc–Lau Basin system and the major tectonic elements therein (VFR – Valu Fa Ridge, ELSC – Eastern Lau Spreading Center, CLSC – Central Lau Spreading Center, NSC – Niuafo'ou Spreading Center, FSC – Fonualei Spreading Center, MTJ – Mangatolu Triple Junction). Shading and scale bar indicate bathymetry.

show systematic changes in source composition with distance from the arc front, trace the possible influence of Samoan plume mantle, and shed fresh light on the dynamics of partial melting in this region.

2. Geological Setting, Previous Work, and Sample Details

[4] Lavas from the active Tonga-Kermadec arc and Lau Basin form a compositional end-member of island arc – back-arc systems. This region experiences the most rapid subduction and back-arc spreading rates on Earth [*Bevis et al.*, 1995]. Back-arc melt extraction has led to the arc-front lavas being highly depleted [e.g., *Ewart et al.*, 1998; *Turner and Hawkesworth*, 1997; *Caulfield et al.*, 2008]. As discussed by *Zellmer and Taylor* [2001], the tectonics of the Lau Basin are complex and thought to involve at least three micro-plates. The Fonualei Spreading Center itself is a nascent series of en échelon ridges that extend north from near Fonualei volcano, on the Tonga arc front, to the Mangatolu Triple Junction in the northeastern Lau Basin (see Figure 1). It is only one of about 5 spreading centers that have developed during opening of the basin over the past 6 Myr. Its evolution is described in detail by *Keller et al.* [2008]. Key to the rationale for the present study is that the Fonualei Spreading Center forms one of two active, magmatic extensional zones that extend obliquely from very close to the arc front (~20 km) into the back-arc. This affords the opportunity to investigate changes in source composition and melting conditions with increasing distance above the slab. U-series data from the other Lau spreading centers

[*Peate et al.*, 2001], provide a useful comparison along with other back-arc systems.

[5] The samples selected for analysis are submarine, basaltic glasses dredged along the Fonualei Spreading Center (Figure 1) during the 2004 research voyage of the Australian Marine National Facility (*R/V Southern Surveyor*). The samples form a subset of a larger suite of samples described in detail, both petrographically and chemically, by *Keller et al.* [2008]. They span a range of calculated depths to the slab (132 to 214 km) and two samples (ND69 and 70) come from the northernmost termination of the Fonualei Spreading Center close to the Mangatolu Triple Junction (see Figure 1). Back-projection of the overall trend of the spreading center intersects the arc front roughly midway between Fonualei and Late Islands (Figure 1).

[6] The major element compositions of the Fonualei Spreading Center lavas are consistent with cotectic crystallization of the observed phenocryst assemblage (olivine, two pyroxenes, plagioclase and chrome spinel). On mantle-normalized, incompatible element diagrams, the samples exhibit positive anomalies for elements like Ba, U, Sr and Pb, that are fluid mobile, and negative Th, Nb-Ta, Zr-Hf and Ti anomalies that render them typical, depleted arc signatures [*Keller et al.*, 2008]. The negative Th, Nb-Ta, Zr-Hf and Ti anomalies mirror those of the pelagic sediment being subducted beneath Tonga [*Turner et al.*, 1997; *Ewart et al.*, 1998; *Plank and Langmuir*, 1998]. The lavas sampled closest to the Mangatolu Triple Junction exhibit a slightly more subdued subduction-related signature and, on the basis of higher S contents, are inferred to be derived from a mantle source region that is significantly more reduced than that of samples dredged further south along the spreading center and sampled along the arc front [*Keller et al.*, 2008].

[7] The mantle wedge in the Tonga – Lau system is notably complex, even prior to subduction modification, and involves both Pacific and Indian MORB as well as plume-influenced sources [e.g., *Hergt and Hawkesworth*, 1994; *Pearce et al.*, 2007; *Falloon et al.*, 2007]. For the modern north Tonga arc and Lau Basin it is now well established that an Indian MORB source is dominant [*Hergt and Hawkesworth*, 1994; *Pearce et al.*, 2007]. The distribution of Samoan plume mantle, as inferred from He and Pb isotopes, has been a source of some controversy [*Wendt et al.*, 1997; *Turner and Hawkesworth*, 1998; *Falloon et al.*, 2007; *Regelous et al.*, 2008; *Lupton et al.*, 2009] and both *Pearce et al.* [2007] and *Turner et al.* [2009] suggested that Hf isotopes may provide an additional discriminate of Indian versus Pacific versus Samoan mantle. Thus, in order to further constrain the distribution of Samoan plume mantle, we also analyzed three boninites from the northern terminus of Tonga trench and two seamounts lying to the north of the trench on the Pacific Plate. The boninites are vesicular porphyritic lavas containing clinopyroxene, orthopyroxene and plagioclase phenocrysts, along with microphenocrysts of clinopyroxene and plagioclase [*Acland*, 1996]. The boninite analyses were performed on whole rocks and the Seamounts on hand-picked glasses. All of these samples are basaltic with high MgO (10–15 wt. %), and are fresh with major element oxide totals between 99.45 and 100.62. Full geochemical data for these samples (from *Acland* [1996]) are provided in Data Set S1 in the auxiliary material along with their locations.[1]

3. Analytical Techniques

[8] H_2O and CO_2 concentrations were analyzed on a Cameca IMS 6f ion microprobe at the Department of Terrestrial Magnetism as part of a study of chalcophile element behavior in the Fonualei Spreading Center lavas (F. Jenner, manuscript in preparation, 2012). Analytical techniques and detection limits were the same as those described in detail by *Hauri et al.* [2002].

[9] The preparation of the submarine glass samples for isotopic analysis employed methods used previously at Macquarie University [see *Beier et al.*, 2010; *Turner et al.*, 2011]. The samples were crushed and then fresh glass chips were handpicked under a binocular microscope. These chips were ultrasonicated for 5 min in a 1:1 solution of 2.5N HCl and 30% H_2O_2. The supernatant was removed and chips were then rinsed in Milli-Q H_2O and ultrasonicated for 10 min before re-picking. Samples analyzed for Sr and Nd isotopes at Macquarie University (ND40, ND58, ND67) were dissolved using a HF-HNO_3 mix in Teflon beakers at 180°C. Sr was isolated by a single pass through Teflon columns containing Biorad® AG50W-X8 (200–400 mesh) cationic exchange resin. The Nd fraction was purified using EIChrom® LN-spec resin according to the method of *Pin and Zalduegui* [1997]. Samples were loaded on to outgassed single (Sr) and double (Nd) rhenium filaments using 2 μl of $TaCl_5$ + HF + H_3PO_4 + H_2O [*Birck*, 1986] and 5 μl of 1N HCl: 0.35N H_3PO_4 activator solutions, respectively. Analyses were performed in static mode on a Thermo-Finnigan Triton® TIMS. Instrumental mass bias was accounted for by normalizing $^{87}Sr/^{86}Sr$ and $^{143}Nd/^{144}Nd$ to $^{86}Sr/^{88}Sr = 0.1194$ and $^{146}Nd/^{144}Nd = 0.7219$, respectively. BHVO-2 served as a procedural standard and yielded $^{87}Sr/^{86}Sr$ of 0.703498 ± 6 and $^{143}Nd/^{144}Nd$ of 0.512975 ± 3. Analysis of the SRM-987 solution yielded an $^{87}Sr/^{86}Sr$ value of 0.710272 ± 4.

[10] Separate dissolutions for Hf isotope analysis of the 3 boninite and 2 seamount samples were carried out at Macquarie University. Hf purification involved decanting the supernatant from an HF dissolution and subsequent isolation using an anionic column followed by a cationic column according to methods described in *Blichert-Toft et al.* [1997]. Hf isotopes were analyzed statically on a Nu Instruments® multicollector, inductively coupled plasma mass spectrometer at Macquarie University following methods described by *Griffin et al.* [2000]. The data were fractionation-corrected to a $^{179}Hf/^{177}Hf$ ratio of 0.7325 and repeat analyses of the JMC475 (n = 7) and BHVO-2 (n = 2) standards during this period yielded $^{176}Hf/^{177}Hf = 0.282178 \pm 6$ (2σ) and 0.283112 ± 16 (2σ), respectively.

[11] All Pb and Hf isotope analyses for the Fonualei Spreading Center lavas, along with the remaining Sr and Nd analyses (samples ND46, ND61, ND62, ND70), were conducted at Durham University. Powders were leached in 3N

[1] Auxiliary materials are available at ftp://ftp.agu.org/apend/jb/2012jb009526.

HCl for 1 h at ~60°C in an ultrasonic bath, and then rinsed twice in Milli-Q H_2O. Powders were dissolved with HF and HNO_3 in Teflon vials on a hotplate at 120°C. Samples were dried and taken up in 16M HNO_3, closed and placed on a hotplate for several hours, then dried. This was then repeated once. The sample residue was then taken up in 3M HNO_3 ready for loading. Strontium was separated using a Sr-spec™ resin column following the procedure reported in *Charlier et al.* [2006], followed by Pb collection from the same column using 0.4 ml 8N HCl. Hafnium and Nd do not have affinity for the resin and so the sample load and initial acid volumes were collected and the Hf and Nd were then separated following the procedures described in detail by *Nowell et al.* [2003] and *Dowall et al.* [2003]. All isotope ratios were measured using a ThermoFinnigan Neptune Multicollector Plasma Mass Spectrometer. Nd was analyzed in a total REE-cut requiring correction for isobaric interferences from Sm on ^{144}Nd, ^{148}Nd and ^{150}Nd. The range of ^{147}Sm/^{144}Nd ratios measured during analysis was ~0.07 to 0.19. The accuracy of the Sm correction method is demonstrated by repeat analyses of BHVO-1, which gave an average ^{143}Nd/^{144}Nd ratio of 0.512982 ± 0.000007 (13.5 ppm 2SD, n = 13) after Sm correction; identical to the TIMS ratio of 0.512986 ± 0.000009 (17.5 ppm 2SD; n = 19) obtained by *Weiss et al.* [2005]. Strontium, Nd, Hf and Pb isotopes were measured in four single analytical sessions (in August 2007) in which the standard solution gave the following means and precision: mean ^{143}Nd/^{144}Nd values for pure and Sm-doped J&M standards were 0.511114 ± 0.000010 (20 ppm 2SD; n = 8) and 0.511115 ± 0.000011 (21 ppm 2SD; n = 7) respectively. Repeat analyses of NBS987 gave a mean ^{87}Sr/^{86}Sr value of 0.710262 ± 0.000015 (22 ppm 2SD; n = 10), while the Hf standard JMC475 gave an average ^{176}Hf/^{177}Hf of 0.282142 ± 0.000007 (24 ppm 2SD; n = 7). Mean values of ^{206}Pb/^{204}Pb, ^{207}Pb/^{204}Pb and ^{208}Pb/^{204}Pb for NBS981 were 16.94134 ± 0.00398, 15.49727 ± 0.00254 and 36.71381 ± 0.00789, respectively (235 ppm, 164 ppm and 215 ppm, 2SD; n = 11). The procedural Pb blanks over the time period of analysis were <20 pg (4–18 pg), with the blank contribution never exceeding 0.015% of the total analyte.

[12] U, Th and Ra concentrations and isotope ratios were determined at Macquarie University on samples that were spiked with ^{226}U-^{229}Th and ^{228}Ra tracers and dissolved using an HF-HNO_3-HCl mix in heated Teflon pressure bombs. The product was converted to chloride using 6N HCl and then 6N HCl saturated with H_3BO_3 to drive-off residual fluorides. The final product was then converted to nitrate using 14N HNO_3 and finally taken up in 7N HNO_3. U and Th purification was achieved via a single pass through a 4 ml anionic resin column using 7N HNO_3, 6N HCl and 0.2N HNO_3 as elutants. We purposefully avoided the use of ElChrom® resins for the U-Th chemistry as these bleed organics that can lead to memory effects and interferences during MC-ICP-MS analysis. Concentrations and isotope ratios were measured in dynamic mode on a Nu Instruments® MC-ICP-MS. ^{238}U and ^{235}U were analyzed on Faraday cups, using the ^{238}U/^{235}U ratio to determine the U mass bias, assuming ^{238}U/^{235}U = 137.88, while ^{236}U and ^{234}U were alternately collected in the IC0 ion counter that is preceded by an energy filter. The IC0 gain was determined during interspersed dynamic analyses of CRM145 assuming a ^{234}U/^{238}U ratio of 5.286×10^{-5} [*Cheng et al.*, 2000]. Methods for Th isotope measurements employed a dynamic routine with ^{232}Th in Faraday cups and ^{230}Th and ^{229}Th alternating on IC0 and using bracketing measurements of the Th"U" standard [*Turner et al.*, 2001b] to obtain the Th mass bias which is different to that for U. Measurements at masses 230.5 and 229.5 were used to derive a correction for residual ^{232}Th tail interference as described in detail in Appendix A of *Sims et al.* [2008] and *Turner et al.* [2011]. Multiple analyses of the secular equilibrium rock standard TML-3 (n = 5) performed at the same time as the samples yielded the following results: U = 10.315 ppm, Th = 29.034 ppm, (^{234}U/^{238}U) = 1.002, (^{230}Th/^{232}Th) = 1.082, (^{230}Th/^{238}U) = 1.004 that are within error of secular equilibrium and published values for this rock [*Sims et al.*, 2008]. See *Beier et al.* [2010] and *Turner et al.* [2011] for the results for other standards and a full discussion of precision and accuracy in this laboratory.

[13] The Ra analysis procedure followed that used by *Turner et al.* [2000]. Ra was taken from the first elution from the anionic column and converted to chloride using 6N HCl. This was then loaded in 3 N HCl onto an 8 ml cationic column and Ra eluted using 3.75M HNO_3 and the process repeated on a scaled-down, 0.6 ml column. The REE were then removed using a 150 μl column of ElChrom® Ln-spec resin™ and 0.1N HNO_3. Ra and Ba were finally chromatographically separated using ElChrom® Sr-spec resin™ and 3N HNO_3 as the elutant in a 150 μl procedure. Samples were loaded onto degassed Re filaments using a Ta-HF-H_3PO_4 activator solution [*Birck*, 1986] and ^{228}Ra/^{226}Ra ratios were measured to a precision typically ~0.5% in dynamic ion counting mode on a ThermoFinnigan Triton® TIMS. Organic interferences are often noted at low temperatures during TIMS analysis for Ra but were limited here by fitting a dry scroll pump instead of the standard rotary pump. This prevents leakage of organic molecules into the source during venting. Accuracy was assessed via replicate analyses (n = 5) of TML-3 that yielded ^{226}Ra = 3532 fg/g and (^{226}Ra/^{230}Th) = 1.02 that is within error of secular equilibrium [see also *Beier et al.*, 2010; *Turner et al.*, 2011]. Because the eruption ages of the samples are unknown, no age correction was applied to any of the U-series data.

4. Results

[14] The full major and trace element data for the samples are available in *Keller et al.* [2008] and only the new results are presented in Table 1 though, for convenience, the whole database (including longitudes and latitudes) may be accessed in Text S1. The samples analyzed here are basalts and basaltic-andesites with SiO_2 = 49 to 55 wt. %. They have H_2O contents that range from 0.89 to 1.23 wt. %. In the case of samples ND40 and 46, the new SIMS H_2O determinations of 1.23 and 1.16%, respectively, are in good agreement with the preliminary FTIR values (1.37 and 1.18 wt.%, respectively) reported by *Keller et al.* [2008] and the water content for sample ND70 (0.95 wt. %) agrees well with long-term average data from the DTM laboratory for this sample of H_2O = 0.95 wt. % (T. Plank, personal communication, 2012). The CO_2 contents range from 1.66 to 107 ppm, though the latter value for sample ND70 is slightly higher than the long-

Table 1. New Data for Fonualei Spreading Center (FSC) and Mangatolu Triple Junction (MTJ) Samples[a]

Sample Number	Water Depth (m)	Depth to Slab (km)	H_2O (wt. %)	CO_2 (ppm)	U (ppm)	Th (ppm)	^{226}Ra (fg/g)	$^{87}Sr/^{86}Sr$	$^{143}Nd/^{144}Nd$	$^{176}Hf/^{177}Hf$	$^{206}Pb/^{204}Pb$	$^{207}Pb/^{204}Pb$	$^{208}Pb/^{204}Pb$	$(^{234}U/^{238}U)$	$(^{238}U/^{232}Th)$	$(^{230}Th/^{232}Th)$	$(^{230}Th/^{238}U)$	$(^{226}Ra/^{230}Th)$
ND46	1340	132	1.16	2.32	0.164	0.216	154	0.703497	0.512978	0.283185	18.588	15.561	38.274	0.998	2.311	1.396	0.604	5.40
ND40[b]	1670	140	1.23	2.29	0.089	0.147	52	0.703526	0.512965	0.283229	18.598	15.562	38.308	0.999	1.830	1.271	0.695	2.43
ND58[b]	1680	151	-	-	0.114	0.189	40	0.703556	0.512941	0.283235	18.603	15.565	38.321	1.007	1.828	1.275	0.698	1.38
ND61	1850	155	1.15	1.66	0.109	0.182	127	0.703586	0.512970	0.283233	18.647	15.562	38.358	0.995	1.822	1.191	0.653	5.19
ND62	1240	155	0.89	2.35	0.137	0.254	109	0.703526	0.512968	0.283230	18.623	15.558	38.326	1.000	1.642	1.200	0.737	3.17
ND67[b]	1750	177	1.07	2.27	0.145	0.303	76	0.703444	0.512929	0.283199	18.619	15.566	38.413	0.992	1.453	1.623	1.117	1.38
ND69	2220	206	1.19	92.63	0.171	0.332	289	0.703905	0.512860	0.283121	18.549	15.576	38.618	0.995	1.564	0.923	0.590	8.27
ND69 rpt.	-	-	-	-	*0.169*	*0.320*	-	-	-	-	-	-	-	*0.993*	*1.601*	*0.928*	*0.584*	-
ND69 rpt.	-	-	-	-	-	-	*291*	-	-	-	-	-	-	-	-	-	-	*8.32*
ND69 rpt.[b]	-	-	-	-	-	-	-	*0.703898*	*0.512851*	*0.283116*	-	-	-	-	-	-	-	-
ND69 rpt.[b]	-	-	-	-	-	-	-	*0.703916*	*0.512852*	-	-	-	-	-	-	-	-	-
ND70	2500	214	0.95	107.11	0.068	0.152	41	0.703803	-	0.283119	18.554	15.572	38.595	0.998	1.351	1.247	0.923	1.90

[a]Major and trace element data for these samples are available in *Keller et al.* [2008]. Italics indicate repeat analyses.
[b]Sr and Nd isotopes analyzed at Macquarie University; otherwise radiogenic isotopes analyzed at Durham University and all U-series isotopes analyzed at Macquarie University.

term average data from the DTM laboratory for this sample of 80 ppm (T. Plank, personal communication, 2012).

[15] $^{87}Sr/^{86}Sr$ and $^{143}Nd/^{144}Nd$ range from 0.703444 to 0.703916 and 0.512851 to 0.512978, respectively. Sample ND69 was analyzed at both Macquarie and Durham Universities to facilitate inter-laboratory comparison and the results indicate good agreement between the two laboratories (Table 1). $^{206}Pb/^{204}Pb$ ranges from 18.549 to 18.647, $^{207}Pb/^{204}Pb$ from 15.558 to 15.576 and $^{208}Pb/^{204}Pb$ from 38.274 to 38.618. The new Fonualei Spreading Center Pb data overlap the field for published data from the arc, as do the samples from the Mangatolu Triple Junction (Figure 2a). $^{176}Hf/^{177}Hf$ ranges from 0.283116 to 0.283235. Figure 2b shows that, overall, these new radiogenic isotope data lie within the ranges previously reported for rocks from the Tonga arc–Lau Basin [*Turner and Hawkesworth*, 1997; *Ewart et al.*, 1998; *Pearce et al.*, 2007; *Hergt and Woodhead*, 2007; *Escrig et al.*, 2009; *Turner et al.*, 2009].

[16] Boninites from the northern Tonga trench and two seamounts on the Pacific Plate have $^{176}Hf/^{177}Hf$ between 0.282724 and 0.283136 (Table 2). When combined with earlier data [*Turner et al.*, 2009], it is clear that the boninites have elevated $^{176}Hf/^{177}Hf$ ratios that are readily distinguishable from the seamounts ($^{176}Hf/^{177}Hf$ = 0.28277–0.28272) that fall at the lower end of the range reported for Samoan basalts [*Pfänder et al.*, 2007; *Jackson et al.*, 2007; *Salters et al.*, 2011]. Note that seamount sample 16–95/2 was also analyzed by *Pearce et al.* [2007] and our new determination is in good agreement with their result ($^{176}Hf/^{177}Hf$ = 0.282731).

[17] U and Th concentrations range from 0.068 to 0.171 and 0.147 to 0.332 ppm, respectively. All of the samples have $(^{234}U/^{238}U)$ ratios that are within analytical error of secular equilibrium (estimated to be 0.08% during this period of analysis [*Beier et al.*, 2010; *Turner et al.*, 2011]. The U-Th-Ra isotope systematics are similar to previously published data from Tonga [*Turner and Hawkesworth*, 1997; *Regelous et al.*, 1997; *Turner et al.*, 2000] and the Lau Basin [*Peate et al.*, 2001]. $(^{238}U/^{232}Th)$ ratios range from 1.351 to 2.311 and $(^{230}Th/^{232}Th)$ from 0.923 to 1.623. The high $(^{230}Th/^{232}Th)$ ratio of 1.623 in sample ND67 appears somewhat anomalous but was duplicated during reanalysis of the same sample solution. For sample ND69 all U-series data replicated within analytical error, except Th concentration, which may reflect true sample heterogeneity. In total, 7 samples have ^{238}U-excess with $(^{230}Th/^{238}U)$ ratios ranging from 0.590 to 0.923 whereas sample ND67 has a ^{230}Th-excess with $(^{230}Th/^{238}U)$ = 1.117.

[18] As the age of the samples is unknown, all of the $(^{226}Ra/^{230}Th)$ ratios must be treated as minimum values. The measured $(^{226}Ra/^{230}Th)$ ratios range from 1.38 to 8.27 – the latter being the highest yet measured from this arc or for any other lava [*Turner et al.*, 2000]. A repeat dissolution and analysis of this sample (ND69) showed excellent reproducibility for the full set of U-series nuclides, including $(^{226}Ra/^{230}Th)$ ratios of 8.27 ± 0.06 and 8.32 ± 0.04 (Table 1). Excepting this sample, the measured $(^{226}Ra/^{230}Th)$ ratios overlap and extend to higher values than those reported for Lau Basin lavas by *Peate et al.* [2001]. In light of the large ^{226}Ra-excesses we conclude that all of the Fonualei Spreading Center lavas are very young (<8 kyr), consistent with their fresh,

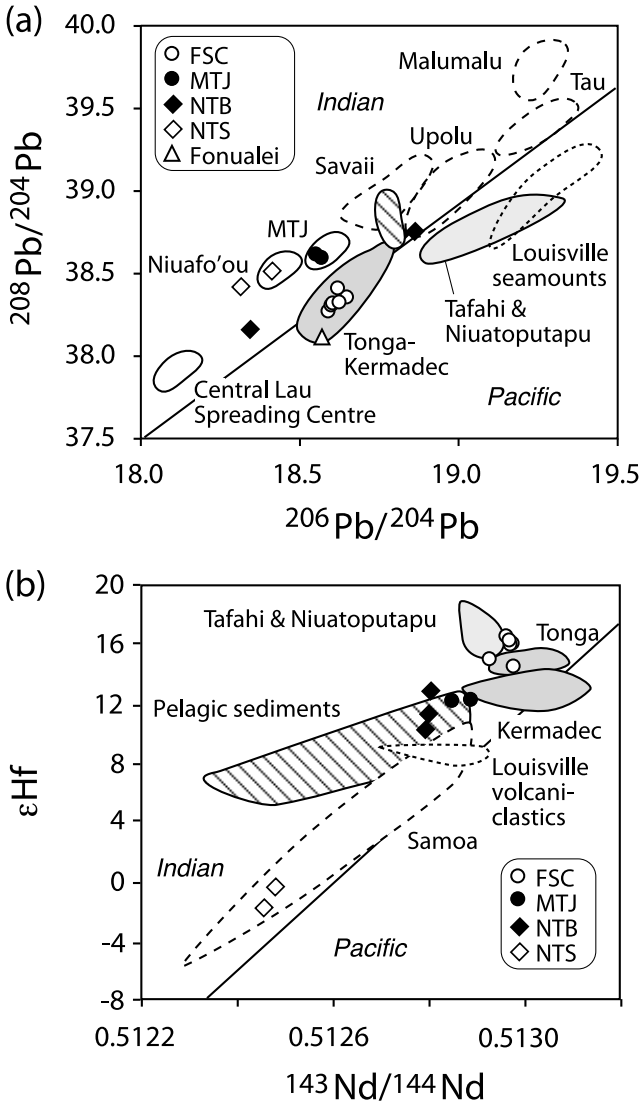

Figure 2. (a) Plot of $^{208}Pb/^{204}Pb$ versus $^{206}Pb/^{204}Pb$ showing the data from this study for the Fonualei Spreading Center and Mangatolu Triple Junction samples (FSC and MTJ) as well as the boninites (NTB) and seamounts (NTS) against fields for the main Tonga-Kermdec arc and the northern islands of Tafahi and Niuatoputapu [*Ewart et al.*, 1998], the Central Lau Spreading Center [*Peate et al.*, 2001], Samoa (dashed fields; data from *Jackson et al.* [2007] and *Workman et al.* [2004]) and the Louisville Seamounts (short-dashed field; data from *Cheng et al.* [1987]) and pelagic sediments (dash-filled field). Fields for Niuafo'ou and other MTJ samples from *Regelous et al.* [2008]. Note the anomalously unradiogenic Pb for one of the boninites (16 26/1). (b) Plot of εHf (calculated assuming chondritic $^{176}Hf/^{177}Hf = 0.282772$) versus $^{143}Nd/^{144}Nd$ showing the data from this study against fields for the Tonga-Kermadec arc rocks, pelagic sediments (dash-filled field), Louisville volcaniclastic sediments and Samoan basalts. Data from *Hergt and Woodhead* [2007], *Pearce et al.* [2007], *Turner et al.* [2009], *Pfänder et al.* [2007], *Salters et al.* [2011] and *Jackson et al.* [2007]. The solid line on both panels separates the fields of *Indian* and *Pacific* MORB according to *Pearce et al.* [2007].

Table 2. Hf Isotopes for Tonga Boninites and Seamounts

Sample Number	Lithology	$^{176}Hf/^{177}Hf$
16-26/1	boninite	0.283091
16-51/8	boninite	0.283136
16-55/4	boninite	0.283067
16-95/2	seamount	0.282724
16-94/1	seamount	0.282767

glassy appearance [*Keller et al.*, 2008]. This also indicates that their ($^{230}Th/^{232}Th$) ratios do not require any age correction.

5. Interpretation

[19] In the following discussion we first map the regional pattern of Hf isotope data to reappraise the distribution of the Samoan mantle plume beneath the Tonga arc – Lau back-arc Basin. We then use the Fonualei Spreading Center data to constrain source component contributions, slab surface temperatures, the conditions of release of slab components and the subsequent mantle melting dynamics for those and other back-arc lavas.

5.1. Extent and Distribution of the Samoan Mantle Plume

[20] *Turner and Hawkesworth* [1998] utilized published He isotope data to suggest that Samoan plume mantle flows southwards into the Lau Basin through the tear in the slab at the northern end of the Tonga arc. However, in contrast to the suggestions of *Wendt et al.* [1997] and *Regelous et al.* [2008], they found no evidence that this material contributes to melting beneath the island arc volcanoes. Samoan basalts have lower $^{176}Hf/^{177}Hf$ and $^{143}Nd/^{144}Nd$ ratios than almost all MORB [*Pfänder et al.*, 2007; *Jackson et al.*, 2007; *Salters et al.*, 2011] and it has been proposed that these isotope systems might also be used to distinguish between plume-affected Lau lavas and the Tonga arc lavas [*Pearce et al.*, 2007; *Turner et al.*, 2009]. Figure 2b shows that the Fonualei Spreading Center lavas lie within the fields for Tonga-Kermadec arc lavas and that those from the Mangatolu Triple Junction have the lowest $^{176}Hf/^{177}Hf$ ratios from this suite. The north Tonga boninites extend to lower $^{176}Hf/^{177}Hf$ and $^{143}Nd/^{144}Nd$ ratios whereas the seamounts markedly have the lowest $^{176}Hf/^{177}Hf$ and $^{143}Nd/^{144}Nd$ ratios measured in this study.

[21] Samoan basalts typically contain ~6 ppm Hf [*Workman et al.*, 2004] and, if they reflect ~5% partial melting, their source can be estimated to have ≪2 ppm Hf. This is more than 20 times higher than estimates for the depleted mantle [*Workman and Hart*, 2005] and so Hf should, in principle, provide a sensitive tracer of Samoan mantle. In Figure 3, we show εHf values, calculated from our new Hf isotope data, as well as published data [*Pearce et al.*, 2007; *Hergt and Woodhead*, 2007], on a map of the Lau Basin – Tonga arc in order to further delineate the extent and distribution of the Samoan mantle plume in this region. We accept that a thorough treatment using multi-isotope space is beyond the scope of this paper and the reader is referred to *Falloon et al.* [2007] for an illustration of the isotopic complexity of the region.

[22] The Samoan basalts have εHf ranging from −5.4 to 10.5 with an average of ~5 [*Pfänder et al.*, 2007; *Jackson et al.*, 2007; *Salters et al.*, 2011]. Therefore, using εHf <

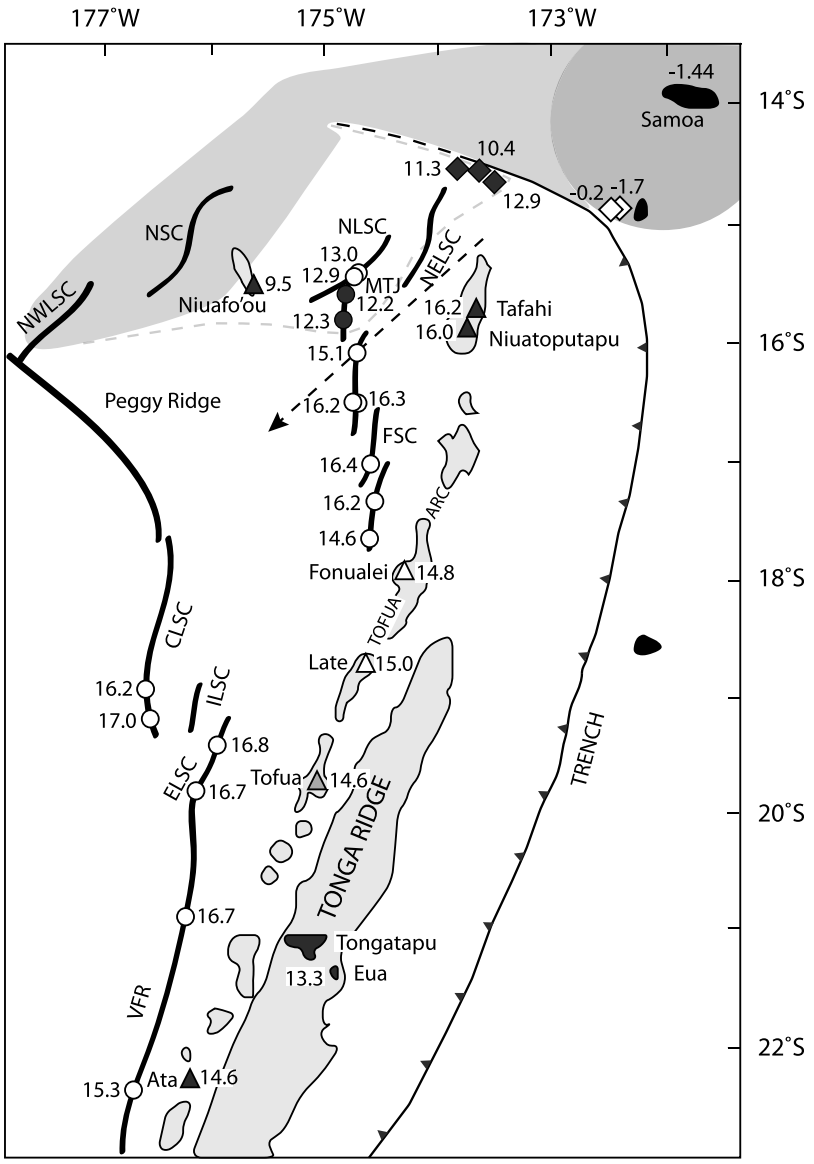

Figure 3. Map of the Tonga arc–Lau Basin system showing εHf numbers for analyzed basalts and the inferred extent of influence from Samoan plume mantle (assuming εHf < 13) that is inferred to influx into the back-arc through a tear in the subducting slab. The dark shaded zone indicates a minimum radius for the Samoan plume based on inclusion of the seamounts within it. The lighter shaded zone is the likely extent of Samoan influence, after interaction with shallow mantle flow, based on He isotope data [*Turner and Hawkesworth*, 1998; *Lupton et al.*, 2009] while the dashed line indicates the possibly larger extent based on Pb [*Regelous et al.*, 2008] and Hf isotope data (sources as for Figure 2). Abbreviations and symbols as in Figures 1 and 2. The new boninite and seamount data suggest that the tear in the slab ceases somewhere in the vicinity of the boninite localities. The arrow indicates the general direction of mantle flow, if the He, Nd and Hf isotope systems become modified by preconditioning (see text for explanation).

13 as a cut-off for plume affected mantle (DMM εHf = 17.3 [*Workman and Hart*, 2005]), Figure 3 shows, from the perspective of Hf isotopes, that the Samoan plume is not present to any significant extent beneath the Fonualei Spreading Center. Samples from the Northern Lau Spreading Center, Mangatolu Triple Junction and Niuafo'ou Island have lower εHf than the Fonualei Spreading Center or Tafahi and Niuatoputapu Islands and Pb isotope data from these localities has been used to infer a limited Samoan influence [*Regelous et al.*, 2008]. In detail, the Pb isotope data for two of the boninites are Samoan in character but the seamounts are more similar to Niuafo'ou and the Mangatolu Triple Junction (Figure 2a). This emphasizes the complexity of the region and *Falloon et al.* [2007] inferred the presence of a number of different plume components in the region.

[23] Notwithstanding these caveats, there is no evidence for elevated $^{3}He/^{4}He$ ratios in lavas east of Niuafo'ou [*Turner and Hawkesworth*, 1998; *Lupton et al.*, 2009]. Instead, the He isotope data would appear to confirm the influence of the Samoan plume beneath the Niuafo'ou and

Northwest Lau Spreading Center further to the west [*Turner and Hawkesworth*, 1998; *Lupton et al.*, 2009]. The boninites from the northern terminus of the Tonga trench have εHf = 10.4 to 12.9, providing evidence for a restricted plume influence whereas the seamounts on the Pacific Plate just to the north of the trench show unambiguous evidence for a Samoan component (εHf = −1.7 to −0.2). These data may be used to infer that the eastward extent of the tear in the Pacific Plate ceases somewhere in the vicinity, or to the west of, the boninite localities, as illustrated in Figure 3.

[24] An alternative explanation, based on *Pearce et al.* [2007], is that "preconditioning" of the mantle raised the $^{176}Hf/^{177}Hf$ ratios. In this model, the Samoan plume contains "plums" of enriched material (e.g., with low $^{176}Hf/^{177}Hf$ ratios) that are preferentially extracted during partial melting such that this mantle loses much of its characteristic isotopic signature as it rises, melts and flows southwestward [*Pearce*, 2005]. This would restrict the utility of the He, Nd and Hf isotope systems as tracers of Samoan plume mantle but could reconcile the high $^{176}Hf/^{177}Hf$ ratios in the Tafahi and Niuatoputapu lavas, so long as they subsequently inherit their radiogenic Pb from the subducting slab. Irrespective of which model is correct for the northern arc islands, all data are consistent with the general direction of mantle flow being south to southwest, along the arc as indicated by the arrow in Figure 3 and as inferred from seismic anisotropy data [*Smith et al.*, 2001].

[25] Intriguingly, the northernmost arc volcanoes of Tafahi and Niuatoputapu have the highest εHf ratios of any of the measured Tonga arc lavas [*Hergt and Woodhead*, 2007; *Pearce et al.*, 2007]. As noted by *Turner et al.* [2009], the elevated εHf ratios of these lavas are not easily reconciled with abundant Pb isotope evidence (see Figure 2a) for a contribution from subducted Louisville seamount sediment [*Wendt et al.*, 1997; *Turner and Hawkesworth*, 1997; *Ewart et al.*, 1998; *Regelous et al.*, 2010]. However, several recent studies have argued that the sediment component observed in many arc lavas is added as a melt formed in equilibrium with residual zircon [*Tollstrup and Gill*, 2005; *Handley et al.*, 2011] and experiments on the pelagic sediments being subducted beneath Tonga were inferred to have produced zircon during melting [*Johnson and Plank*, 1999]. Therefore, one possible solution to this dilemma is that the Louisville Pb signature was carried by a wet sediment melt that formed in the presence of residual zircon that retained the majority of the Hf from this component [*Turner et al.*, 2009]. This would enable the Louisville signature to be transferred in Pb isotopes but not in Hf isotopes and the Tafahi and Niuatoputapu lavas have distinct negative Zr-Hf anomalies on mantle-normalized, incompatible trace element diagrams [*Turner et al.*, 1997], consistent with the presence of residual zircon.

5.2. Slab Contributions to the Source of the Fonualei Spreading Center Lavas

[26] *Keller et al.* [2008] showed that Fonualei Spreading Center lavas have typical arc signatures. These include low Ce/Pb and elevated U/Th and Th/Nb [e.g., *Gill and Williams*, 1990; *Hawkesworth et al.*, 1993; *Miller et al.*, 1994; *Pearce et al.*, 1995; *Ewart et al.*, 1998; *George et al.*, 2003; *Bézos et al.*, 2009] and often elevated Sm/Zr [*Handley et al.*, 2011]. Wet sediment melts have all of these characteristics [e.g., *Johnson and Plank*, 1999; *Hermann and Rubatto*, 2009] while the strongly fluid mobile nature of Pb and U^{6+} [e.g., *Brenan et al.*, 1995; *Stalder et al.*, 1998] provides an additional mechanism for explaining low Ce/Pb coupled with high U/Th in arc lavas. Sediments also have high $^{87}Sr/^{86}Sr$ and $^{208}Pb/^{204}Pb$ coupled with low $^{143}Nd/^{144}Nd$ that could be transferred into the mantle wedge. In contrast, Tongan slab fluids are inferred to be derived from subducted, altered oceanic crust and to have lower $^{87}Sr/^{86}Sr$ and $^{208}Pb/^{204}Pb$ ratios of ~0.7035 and ~37.7, respectively [e.g., *Turner et al.*, 1997, 2012; *Castillo et al.*, 2009; *Escrig et al.*, 2009].

[27] Using these indices, we appraise variations in the contributions of slab-derived fluids and/or sediment components to the source of the Fonualei Spreading Center lavas. Aqueous fluid-sensitive trace element ratios, such as Ce/Pb and U/Th (Figures 4a and 4b), as well as Ba/Th, Sr/Th (not shown) all decrease with distance from the arc front (represented by an average basaltic-andesite from Late Island in Figure 4). This is consistent with models in which progressive dehydration of the slab leads to a decreased overall fluid flux with distance from the arc [e.g., *Schmidt and Poli*, 1998]. However, the absolute H_2O contents of the lavas do not vary systematically with distance (see Table 1 and *Keller et al.* [2008]) and therefore it may be that it is the concentration of fluid-mobile, trace elements in the fluid that decreases, rather than the absolute amount of H_2O (for example, K_2O/H_2O ranges from 0.25 to 0.68). This could reflect either progressive depletion of Ba, U, Sr and Pb in the residual slab or variations in the partitioning and buffering of these elements due to changes in the residual mineral assemblage that occur with increasing temperature [*Hermann and Rubatto*, 2009]. Alternatively, melt productivity may be linearly tied to H_2O flux.

[28] Experimental data indicate that wet sediment melts are likely to carry a much higher inventory of incompatible elements compared with slab-derived, aqueous fluids [*Spandler et al.*, 2007; *Hermann and Rubatto*, 2009]. Ratios of non-supercritical, aqueous fluid-immobile trace elements, such as Th/Nb and Sm/Zr, can be employed as tracers of contributions from subducted sediment, or sediment melts, because pelagic sediments (and thus sediment melts) have high Th/Nb and Sm/Zr relative to the mantle [e.g., *Plank and Langmuir*, 1998]. Because these ratios involve elements of similar compatibility they are thus much more sensitive to sediment addition than to source heterogeneity or partial melting. It can be seen from Figure 4d that Th/Nb ratios decrease continuously with distance from the arc. Because Nb/Ta ratios are essentially constant in these lavas (~15), implying a small but uniform prior depletion of the mantle wedge [*Caulfield et al.*, 2008], we attribute this decrease in Th/Nb to a decreasing sediment contribution. A combination of decreasing sediment and aqueous fluid contributions can also explain the trends for both Ce/Pb and U/Th in Figure 4. We note that Sm/Zr shows a more complex behavior, initially increasing and then decreasing with distance from the arc front (not plotted). Since the bulk sediment composition is unlikely to change along this path this reflects more complex behavior (see further discussion below).

[29] Assuming a broadly constant, pre-subduction modified mantle wedge composition, a decreasing contribution from fluids/sediment melts should result in decreasing $^{87}Sr/^{86}Sr$ and increasing $^{143}Nd/^{144}Nd$, as observed along the Valu Fa Ridge for example, but this is not the case here

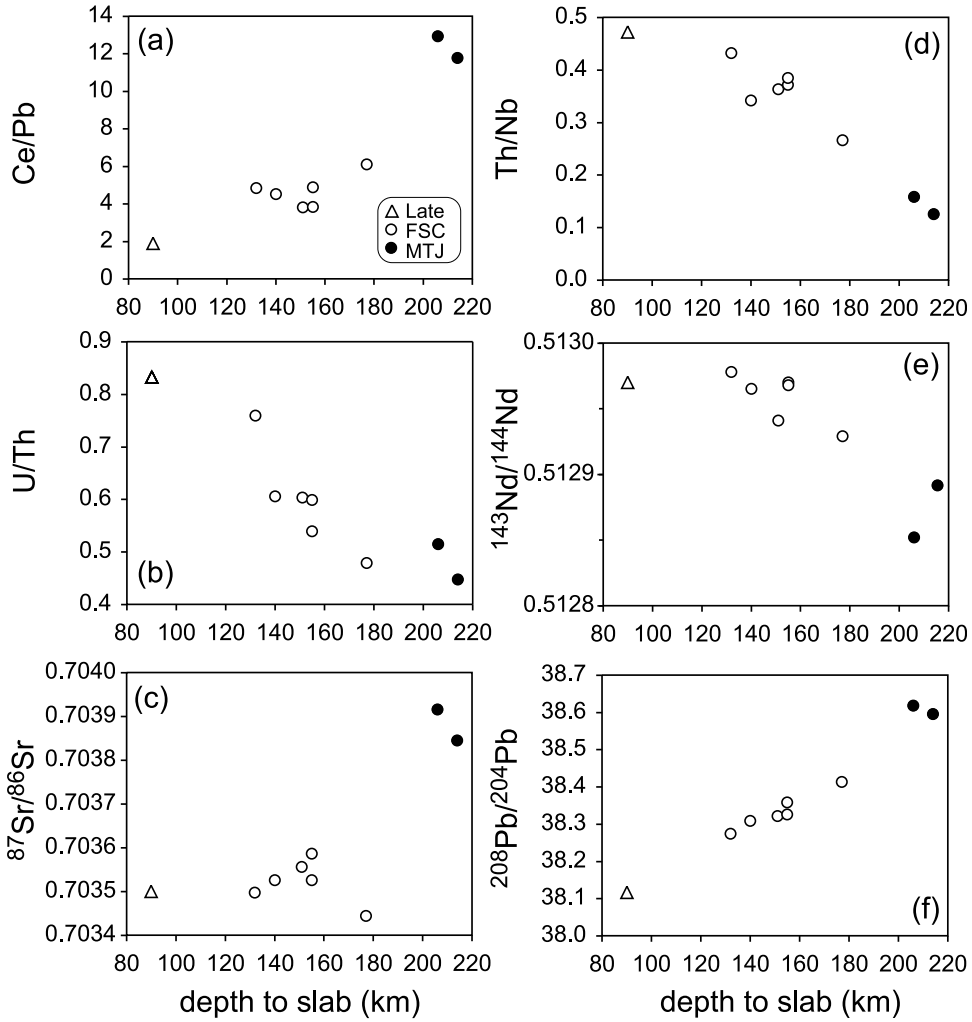

Figure 4. (a–f) Plots of selected, component-sensitive geochemical parameters against depth to slab for the Fonualei Spreading Center samples and an average basaltic-andesite from Late Island which is plotted to provide a reference point for the arc front (data from *Turner et al.* [1997]). See text for discussion.

(Figures 4c and 4e). Previous work has shown that lavas from the Mangatolu Triple Junction and Niufo'ou Island are characterized by $^{87}Sr/^{86}Sr \sim 0.704$ and $^{143}Nd/^{144}Nd \sim 0.5128$ [*Regelous et al.*, 2008]. Therefore, these isotope trends are likely influenced by an increasing contribution from plume-like northeastern Lau Basin mantle *as well as* by changes in slab contributions. As discussed above, the extent to which this reflects the influence of the Samoan plume remains open to debate. For example, it is well documented that Pb isotope systematics in the region are complex, requiring at least three or, arguably, four component mixing for the arc and back-arc lavas [*Turner et al.*, 1997; *Ewart et al.*, 1998; *Falloon et al.*, 2007; *Regelous et al.*, 2010]. $^{208}Pb/^{204}Pb$ increases linearly along the Fonualei Spreading Center (Figure 4f) and the lower values near the arc front are consistent with addition of a slab fluid that lowered the Ce/Pb ratios in Figure 4a and had $^{208}Pb/^{204}Pb \sim 37.7$ [*Turner et al.*, 2012]. However, while the Fonualei Spreading Center lavas form an array broadly consistent with other central Tonga lavas [e.g., *Regelous et al.*, 2010], the Mangatolu Triple Junction lavas have lower $^{206}Pb/^{204}Pb$ despite their higher $^{208}Pb/^{204}Pb$ (Figure 2a). This is similar to other lavas from the triple junction and Niuafo'ou Island and likely reflects mixing between Indian MORB mantle typical of the Central Lau Spreading Center and Samoan mantle (see Figure 2 and *Regelous et al.* [2008]). There have been numerous attempts at quantitative modeling of the trace element and isotope trends in this region [*George et al.*, 2005; *Hergt and Woodhead*, 2007; *Falloon et al.*, 2007; *Escrig et al.*, 2009; *Regelous et al.*, 2010] and so, rather than revisit these calculations, we focus instead on comparing inferences on the thermal state of the slab with recent experimental data and the implications of the U-series isotopes for melting dynamics.

5.3. Slab Surface Temperatures and the Conditions of Slab Component Release

[30] A number of recent studies have used both published FTIR and SIMS analyses of the H_2O contents of submarine, back-arc glasses to investigate the role of H_2O in back-arc melting systematics [e.g., *Taylor and Martinez*, 2003; *Langmuir et al.*, 2006; *Kelley et al.*, 2006; *Bézos et al.*, 2009, and references therein]. A general concern with this approach is the extent to which such glasses may have degassed. CO_2 begins degassing before H_2O and Table 1

shows that the Fonualei Spreading Center lavas only retain 1–3 ppm CO_2 indicating the majority has been lost. However, in a detailed study of the Mariana arc and back-arc, *Newman et al.* [2000] showed that, although their basaltic glasses had typically undergone significant loss of CO_2, comparison with melt inclusions indicated that there was minimal disturbance of H_2O. While some deep-level degassing cannot be precluded (and the measured H_2O contents are therefore minima) a commonly accepted approach to date has been to accept data from glasses that would have been H_2O under-saturated at their pressure of eruption. For example, *Langmuir et al.* [2006] used a H_2O saturation curve for basalt with 49 wt. % SiO_2 at 1150°C for this purpose. Because higher SiO_2 contents lead to higher solubility and almost all back-arc basalts have SiO_2 contents greater than this, the saturation curve is taken to be conservative. As shown in Figure 5a, all but one of the new Fonualei Spreading Center lavas (SiO_2 = 49–55 wt. %) lie above the H_2O saturation curve. Except for this sample, the lavas appear to be water-undersaturated, and therefore, the water contents are likely unaffected by degassing and the H_2O/Ce ratios probably represent magmatic values. Therefore, in keeping with previous studies, we infer that these data provide useable constraints on the H_2O contents of these samples. Interestingly, the Mangotolu Triple Junction samples contain significant CO_2 (93 and 107 ppm) and so should not have degassed H_2O. Despite this one of these still falls on the H_2O saturation curve (Figure 5a).

[31] It is well established that H_2O and Ce have similar partitioning behavior during mantle melting [e.g., *Michael*, 1988; *Hauri et al.*, 2006] yet Figure 5b shows that H_2O/Ce ratios decrease away from the arc front. *Plank et al.* [2009] have proposed that H_2O/Ce ratios in arc lavas reflect slab surface temperatures and the effect of residual accessory phases formed during hydrous partial melting of subducting sediments. Accordingly, a logical interpretation is that the trend in Figure 5b reflects increases in slab surface temperatures that are anticipated to develop as slab depth increases. Applying the geothermometer of *Plank et al.* [2009], the H_2O/Ce ratios in the arc front lavas [*Caulfield et al.*, 2012; *Cooper et al.*, 2012] and Fonualei Spreading Center lavas (835–1800) result in calculated slab surface temperatures that increase from ~720°C beneath the arc front to ~866°C at 214 km depth. For the arc front, these estimates are in good agreement with those predicted by recent geophysical models [*Syracuse et al.*, 2010; *Cooper et al.*, 2012] yet they are significantly hotter beyond the front at greater depth. Until independent constraints become available, these temperatures must be treated with caution because any deep-level degassing of H_2O would lead to higher inferred temperatures, although the Mangatolu Triple Junction lavas that have retained CO_2 (and S [*Keller et al.*,

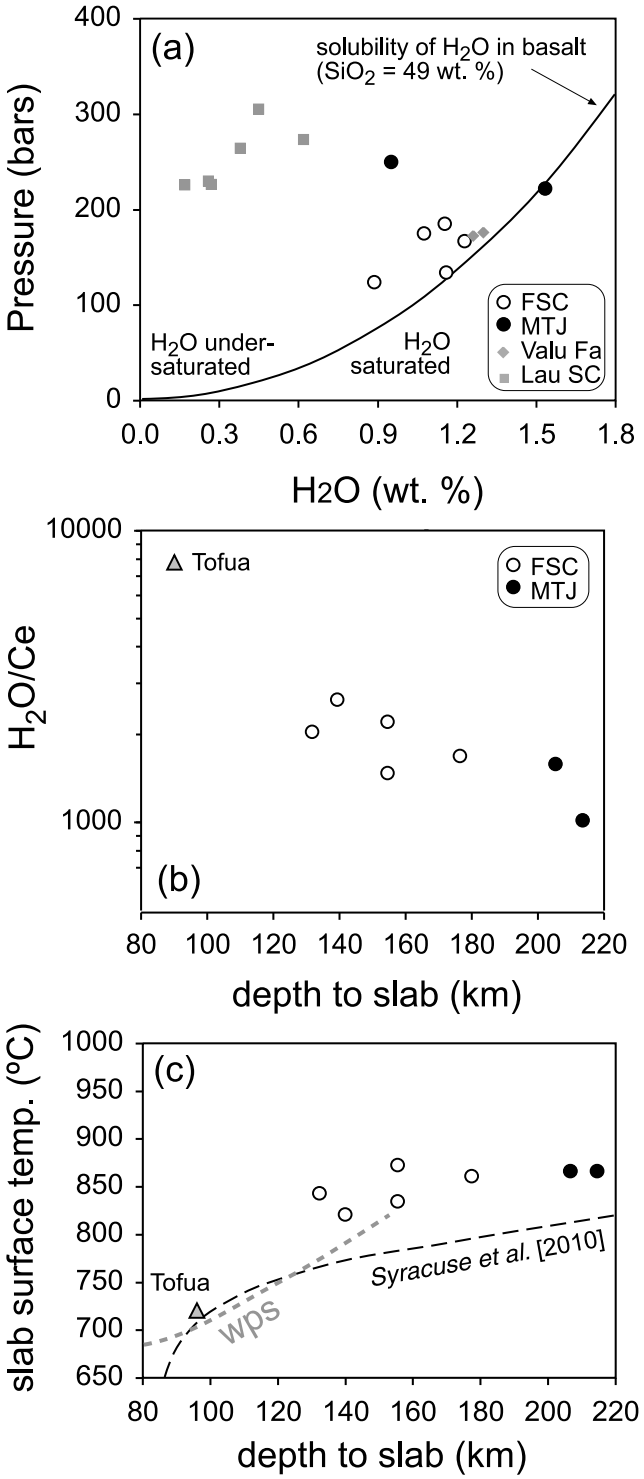

Figure 5. (a) H_2O content versus pressure of recovery for glasses from Fonualei Spreading Center and Lau Basin lavas (data from *Kent et al.* [2002]) with MgO > 6 wt. % and for which U-series data are available. The curve is the H_2O- saturated line for basaltic melts with 49 wt. % SiO_2 at 1150°C [after *Newman and Lowenstern*, 2002]. The implication is that the majority of samples would have been water undersaturated at the depth of recovery and so the measured H_2O contents provide a reasonable minimum estimate of primary magmatic H_2O. (b) H_2O/Ce versus depth to slab for the Fonualei Spreading Center samples and a Tofua basaltic-andesite as representative of the arc front [*Caulfield et al.*, 2012; *Cooper et al.*, 2012]. (c) Slab surface temperature inferred from H_2O/Ce after *Plank et al.* [2009] versus depth to slab. Note that any loss of H_2O due to degassing would erroneously high temperatures. Also shown are the profile of slab surface temperatures from the D80 geophysical model of *Syracuse et al.* [2010] and the composite wet pelite solidus (wps) from *Hermann and Rubatto* [2009].

2008]) also lie above the *Syracuse et al.* [2010] curve in Figure 5c. In addition, *Stepanov et al.* [2012] have found that monazite solubility, on which the geothermometer is calibrated, changes with increasing pressure. Therefore, for the remainder of the discussion we will assume slab surface temperatures based on the *Syracuse et al.* [2010] profile in Figure 5c, but note that there is some evidence the actual temperatures might be higher.

[32] Irrespective of the absolute temperatures, it is reasonable to assume that the slab surface temperatures increase with increasing depth and it is important that the inferred temperatures lie very close to the wet pelite solidus of *Nichols et al.* [1994] and *Hermann and Spandler* [2008] near the arc front (Figure 5c). This is in good accord both with inferences from Tonga arc front melt inclusions [*Plank et al.*, 2009] and with previous studies that have argued that the sediment component was added as a partial melt beneath the Tonga arc [e.g., *Turner and Hawkesworth*, 1997; *Johnson and Plank*, 1999; *George et al.*, 2005]. The wet pelite solidus is not constrained beyond 4.5 GPa and may be higher than the slab surface temperatures (Figure 5c). However, supercritical fluids may become more relevant under these, higher pressure, conditions [*Manning*, 2004; *Kessel et al.*, 2005].

[33] Recently, *Hermann and Spandler* [2008] and *Hermann and Rubatto* [2009] have undertaken an experimental study of sediment melting under conditions appropriate to the temperature-depth profile inferred for the Fonualei Spreading Center lavas in Figure 5c. The results show that the trace element inventory in wet pelite melts evolves progressively with the changes in the mineralogy of the residual assemblage that occur in response to increasing temperature and pressure. Although there are significant differences for many trace element concentrations and ratios between the pelite used in the starting composition for their experiments and the pelagic sediments that subduct beneath Tonga [*Turner et al.*, 1997; *Ewart et al.*, 1998; *Johnson and Plank*, 1999], the Ba and La concentrations of the natural and experimental compositions do match closely, permitting direct comparison. Figure 6a shows that Ba/La ratios decrease with increasing temperature in the experimental melts. Strikingly, this trend is closely matched by the lavas from Fonualei Spreading Center, Valu Fa and Lau Spreading Centers (Figure 6a). The implication is that at least this element ratio is dominantly controlled by wet sediment melt addition.

[34] To further constrain the nature of the sediment component, we utilized the dehydration and partial melting experiments that *Johnson and Plank* [1999] conducted on the Tonga

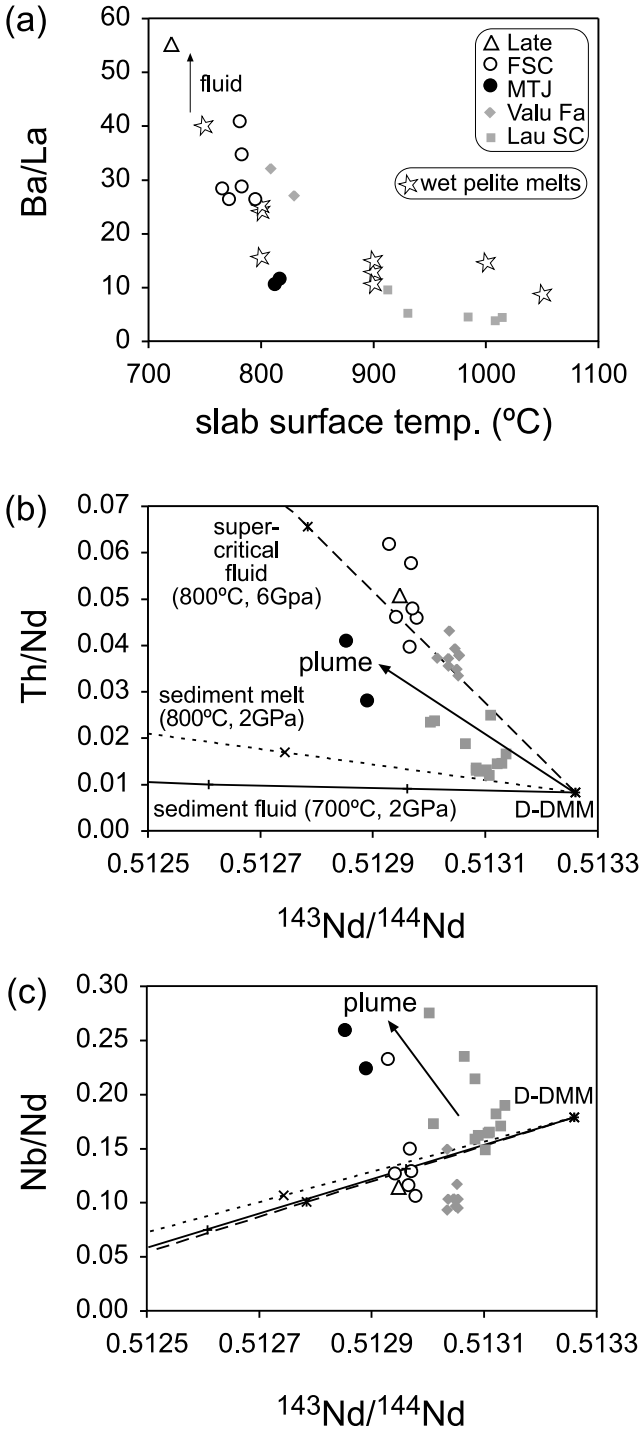

Figure 6. (a) Ba/La versus slab surface temperature (which was taken from the *Syracuse et al.* [2010] curve in Figure 5c) comparing the Fonualei Spreading Center data with experimental, wet pelite melts at the same conditions [*Hermann and Rubatto*, 2009]. Plotted for comparison are data from Lau Basin samples [*Peate et al.*, 2001] with slab-surface temperatures calculated from their H_2O/Ce ratios (only for samples with MgO > 6 wt. % and for which U-series data are available) using the geothermometer of *Plank et al.* [2009] and H_2O and Ce data from *Kent et al.* [2002] and *Peate et al.* [2001]. (b) Th/Nd versus $^{143}Nd/^{144}Nd$ with mixing trajectories toward fluid and melt produced by experiments (conditions indicated) on the Tonga sediment [*Johnson and Plank*, 1999]. Also shown is the trajectory toward a super-critical fluid from the Tonga sediment calculated using the 800°C, 6 GPa partition coefficients of *Kessel et al.* [2005], the average Tonga sediment composition from *Plank and Langmuir* [1998] and assuming F = 0.18 [*Kessel et al.*, 2005]. Increment along curves is for 0.2% addition of the sediment component. (c) Nb/Nd versus $^{143}Nd/^{144}Nd$ with mixing curves as in Figure 6b. The majority of the lavas plotted are inferred to have had a sediment melt or super-critical fluid added to their source regions whereas those from the Mangatolu Triple Junction and some from the Lau Spreading Centers are additionally influenced by a plume component.

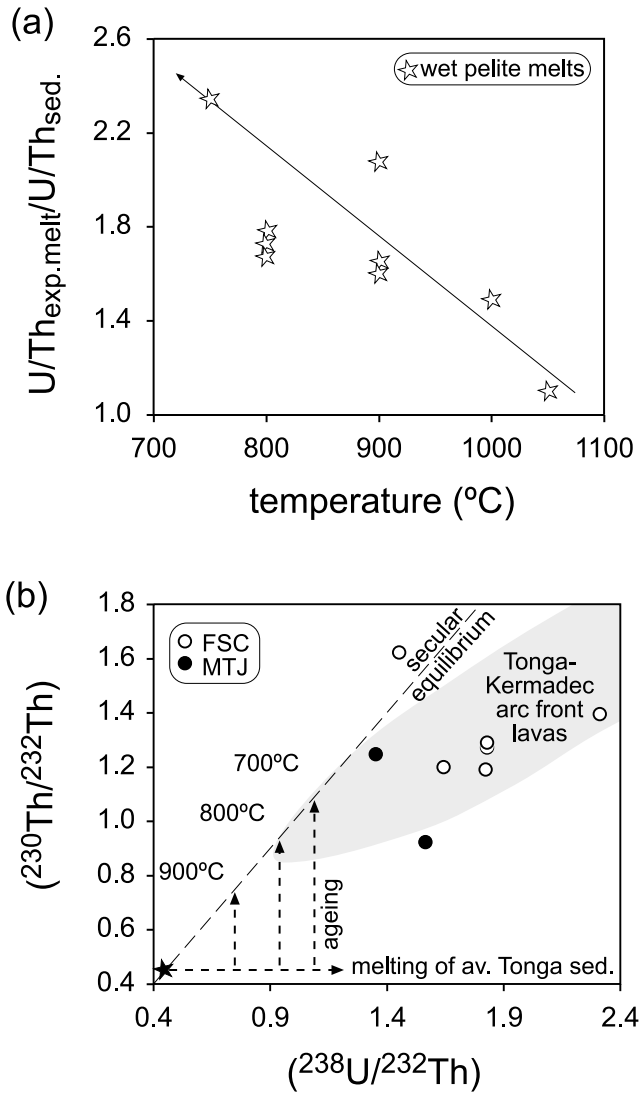

Figure 7. (a) Extent of U/Th fractionation in experimental, wet pelite melts [*Hermann and Rubatto*, 2009] showing that the maximum fractionation occurs at the lowest temperatures. (b) U-Th equiline diagram showing the Fonualei Spreading Center lavas lie at the lower end of the field for mafic to intermediate (SiO_2 < 60 wt. %) Tonga-Kermadec arc lavas [*Turner et al.*, 1997]. Dashed arrows indicate the trajectories of ($^{238}U/^{232}Th$) ratios, inferred from Figure 7a, of melts of an average Tonga pelagic sediment (shown as black star; data from *Plank and Langmuir* [1998]). Assuming that the melts decay back to the equiline [*Turner and Hawkesworth*, 1997], the arc front lava array suggests that the sediment melt was formed between 700 and 800°C. Subsequent addition of U by fluids with or without aging results in the observed ^{238}U excesses.

pelagic sediment. In addition, because the P-T conditions inferred from Figure 5c may exceed the sediment solidus and approach those of super-critical fluids, we have also calculated the composition of a super-critical fluid derived from the Tonga sediment using the 800°C, 6 GPa partition coefficients from the experiments of *Kessel et al.* [2005]. As shown in Figure 6b, the data appear most consistent with addition of the sediment component as either a sediment melt (cf. Figure 6a) or a super-critical fluid derived thereof but not a sediment fluid. *George et al.* [2005] similarly argued that the Tonga-Kermadec lavas showed good evidence for addition of both a sediment melt and an aqueous fluid from altered oceanic crust but no evidence for a sediment-derived fluid [cf. *Class et al.*, 2000]. Figure 6c confirms that some of the more distal back-arc lavas from the Mangatolu Triple Junction and the Eastern Lau Spreading Center additionally are influenced by a plume component (cf. Figures 2a and 3). Finally, some elemental ratios are likely to be strongly controlled by key accessory phases. For example, it seems likely that the inflection in Sm/Zr ratios in the Fonualei Spreading Center lavas reflects the varying role of residual zircon versus monazite and/or allanite in these melts as the slab surface temperature increases. This is consistent with inferences from other arcs [*Tollstrup and Gill*, 2005; *Handley et al.*, 2011] as well as the suggestion, offered above, that residual zircon might explain the Hf isotope dilemma of the north Tonga arc lavas.

[35] In detail, the absolute Ba/La values of the Fonualei Spreading Center, Mangatolu Triple Junction and Valu Fa lavas closely match those from the experiments at the intermediate temperature end of the arrays in Figure 6a whereas those from the Central and Eastern Lau Spreading Centers match the higher temperature experiments. There may be some divergence to higher Ba/La ratios as the cooler conditions beneath the arc front are approached (see Figure 6a) and this most likely reflects augmentation of the Ba flux by aqueous fluids from the slab [e.g., *Pearce et al.*, 1995; *Turner et al.*, 1997]. In an analogous manner, the U/Th ratios of the Tonga pelagic sediment are much lower than those observed in any of the arc front or back-arc lavas. U/Th ratios typically increase during partial melting of pelagic sediments and Figure 7a shows that this fractionation increases with decreasing temperature. *Turner et al.* [1997] showed that the Th budget of the Tonga lavas is dominated by the sediment contribution and argued that the intersection of the arc lava array with the U-Th equiline (see Figure 7b) requires addition of a sediment melt >350 kyr ago such that the melt also attains elevated ($^{230}Th/^{232}Th$) by in-growth [*Elliott et al.*, 1997]. As illustrated on Figure 7b, the experimental data indicate that this will occur if the slab surface temperature beneath the arc front is in the range 700–800°C. This in excellent agreement with the inferences made from Figures 5b and 5c. Subsequent fluid addition results in the ^{238}U and ^{226}Ra excesses that typify the arc front lavas [*Gill and Williams*, 1990; *Regelous et al.*, 1997; *Turner et al.*, 1997, 2000].

5.4. Fluid-Fluxed Versus Decompression Melting

[36] Although all of the lavas exhibit strong island arc signatures, there has been much recent discussion over the relative roles of fluid-fluxed versus decompression melting in the production of back-arc basin basalts [*Kelley et al.*, 2006; *Langmuir et al.*, 2006; *Beier et al.*, 2010]. The rate of spreading increases from 47 to 94 mm/yr northward along the Fonualei Spreading Center [*Keller et al.*, 2008] and this could lead to a faster upwelling rate and a corresponding decrease in extent of U-series disequilibria (see below). Figure 8a is a plot of Ba versus Yb that may potentially discriminate between these two melting processes [cf. *Peate et al.*, 2001]. During decompression melting the concentrations of both highly incompatible (Ba) and mildly

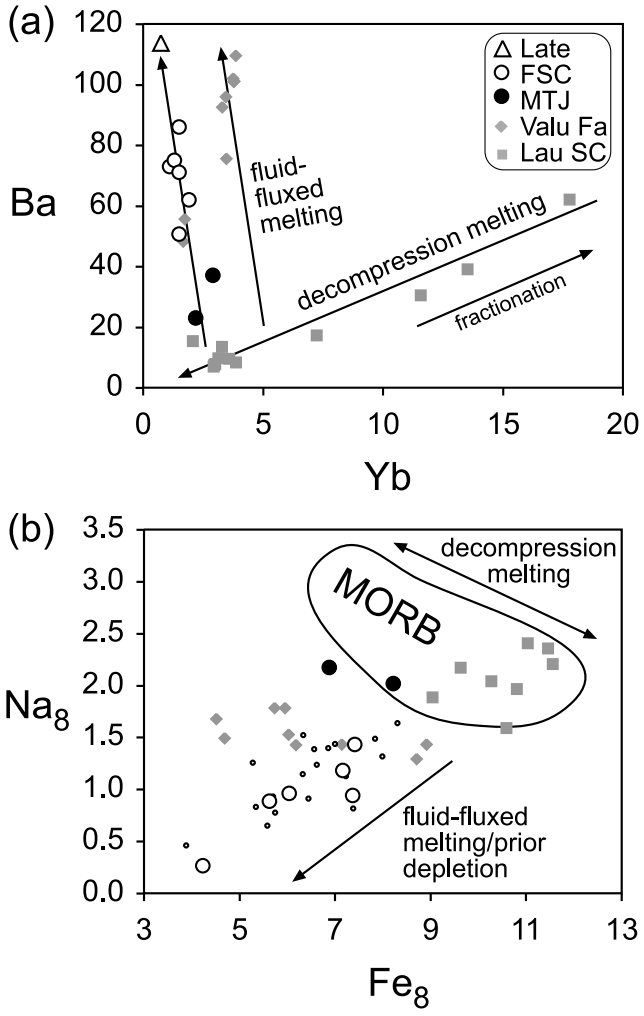

Figure 8. Plots to potentially discriminate between fluid-fluxed and decompression melting. (a) Ba versus Yb [after *Peate et al.*, 2001]. During decompression melting both Ba and Yb concentrations decrease as the extent of melting increases whereas, during fluid-fluxed melting, addition of the fluid leads to increases in Ba coupled with increases in the overall extent of melting that cause dilution of the concentrations of Yb. Note that while some of the range in Ba and Yb in the Lau lavas is attributable to fractionation, the lower Yb and higher Ba in the Valu Fa lavas cannot be a fractionation effect. (b) Na_8 versus Fe_8 (calculated following *Klein and Langmuir* [1987]) for Lau Basin lavas with MgO > 6 wt % and for which U-series data are available. Fonualei Spreading Center data (small dots) from *Keller et al.* [2008]. Mid-ocean ridge basalt (MORB) field from *Klein and Langmuir* [1987]. The positively sloped arrays for the Fonualei Spreading Center and Valu Fa data are similar to those found by *Langmuir et al.* [2006] and *Bézos et al.* [2009] and modeled as mixtures between "dry" (i.e., decompression) and "wet" (i.e., fluid-fluxed) melts.

incompatible (Yb - there is no evidence for residual garnet in these lavas) elements decrease as the extent of melting increases. By contrast, during fluid-fluxed melting addition of the fluid (±sediment component) leads to increases in Ba (cf. Figure 5c) coupled with increases in the overall extent of melting that causes dilution of the concentrations of fluid immobile elements like Yb. Thus, decompression melting should result in positive Ba – Yb trends whereas fluid-fluxed melting should result in a negative trend. As Figure 8a shows, lavas from the Fonualei Spreading Center and Valu Fa Ridge overall form steep negative trends indicative of fluid-fluxed melting whereas lavas sampled further west from the Central and Eastern Lau Spreading Centers form a positive trend consistent with dominance by decompression melting. Similarly, the lavas from the Fonualei Spreading Center and Valu Fa Ridge form a shallow positive trend on a plot of Na_8 versus Fe_8 (Figure 8b). Such trends are typical for back-arcs and have been argued to be consistent with fluid-fluxed melting and/or prior depletion [e.g., *Taylor and Martinez*, 2003; *Langmuir et al.*, 2006]. In contrast, the lavas from the Central and Eastern Lau Spreading Centers overlap the field for mid-ocean ridge basalts that are formed by decompression melting (Figure 8b). The relationships in Figure 8 and the U-series data (see below) provide evidence that lavas from the Mangatolu Triple Junction may have been formed by a combination of these two melting processes.

[37] The cause of melting can be further evaluated using U-series isotopes because decompression melting, in the absence of fluid-fluxing, typically results in excesses of ^{230}Th over ^{238}U [e.g., *McKenzie*, 1985]. In contrast, arc lavas usually have the opposite sense of disequilibria and this is usually attributed to the mobility of U during fluid-fluxing from the slab [e.g., *Gill and Williams*, 1990]. The U-Th isotope data are shown on a U-Th equiline diagram in Figure 7b. All the samples, except ND67, have ^{238}U excesses ranging in magnitude from 8 to 68%. These are similar to many of the Tonga arc front lavas [*Gill and Williams*, 1990; *Turner et al.*, 1997; *Regelous et al.*, 1997] and generally exceed those reported from other Lau Basin lavas [*Peate et al.*, 2001], even though some of the latter were sampled at similar distances from the arc front along the Valu Fa Ridge further to the south (see Figure 1). Like U, Ra is strongly fluid mobile and the Fonualei Spreading Center lavas all have large ^{226}Ra excesses (Table 1). While an unknown amount of ^{226}Ra decay may have occurred since eruption, the magnitude of these excesses (38 to 700%), the inverse correlation with (^{230}Th/^{238}U), and their overlap with the arc front lavas in Figure 9a are features entirely consistent with fluid-fluxed melting [*Turner et al.*, 2000]. The same applies to the Valu Fa lavas. In light of the implications from Figure 8, it is not apparent why sample ND69, from the Mangatolu Triple Junction, has the largest ^{238}U and ^{226}Ra excess of all of the lavas (but see below). Further U-series analyses of samples from this complex region are required to resolve this.

[38] Only sample ND67 from the Fonualei Spreading Center has ^{230}Th excess and this is combined with a moderate ^{226}Ra excess rendering the U-series signature of this sample typical of melts formed by decompression [e.g., *Lundstrom*, 2003]. Note that sample ND67 also has an anomalously high (^{230}Th/^{232}Th) ratio compared with these latter lavas (see Figure 9a) and we are cautious about attributing much significance to this one sample.

[39] In contrast to lavas from the arc front, Fonualei Spreading Center and Valu Fa Ridge, lavas sampled further to the west, from the Eastern Lau Spreading Center, have lower H_2O contents [*Kent et al.*, 2002] and were erupted

where inferred slab surface temperatures are hotter (see Figure 9b). These lavas and those from Niuafo'ou Island [*Regelous et al.*, 2008] (not plotted) typically have ^{230}Th excesses and small ^{226}Ra excesses (Figure 9a). Such signatures are attributed to a much greater contribution from decompression melting [*Peate et al.*, 2001; *Regelous et al.*, 2008] and, overall, there appears to be good consistency between the *inferences* about melting processes derived from the Ba-Yb, Na_8-Fe_8 and the U-series systematics. However, because U-series disequilibria are affected by both fluid addition and melting dynamics, the relatively simple correlations between indices like Ba/Th and ^{226}Ra excess observed in along-arc studies [e.g., *Turner et al.*, 2000], are not apparent in the cross-arc data. The inferred change in melting dynamics could reflect reduced fluid flux from the slab and in both Figures 8 and 9 the transition from inferred fluid-flux-dominated to decompression-dominated melting seems to occur when the slab surface temperatures exceed ~850°C (Figure 8b). For the moment, the cause of this transition remains speculative (see below). Phengite, the last major hydrous phase in altered basalt, becomes unstable around these temperatures at pressures corresponding to ~200 km depth [e.g., *Schmidt and Poli*, 1998]. However, expiry of phengite should result in a flux of Ba yet the associated lavas have the lowest Ba/La ratios (Figure 6a). Instead, the transition could coincide with the expiry of lawsonite, consistent with available B/Be data and recent experimental work [*Martin et al.*, 2011].

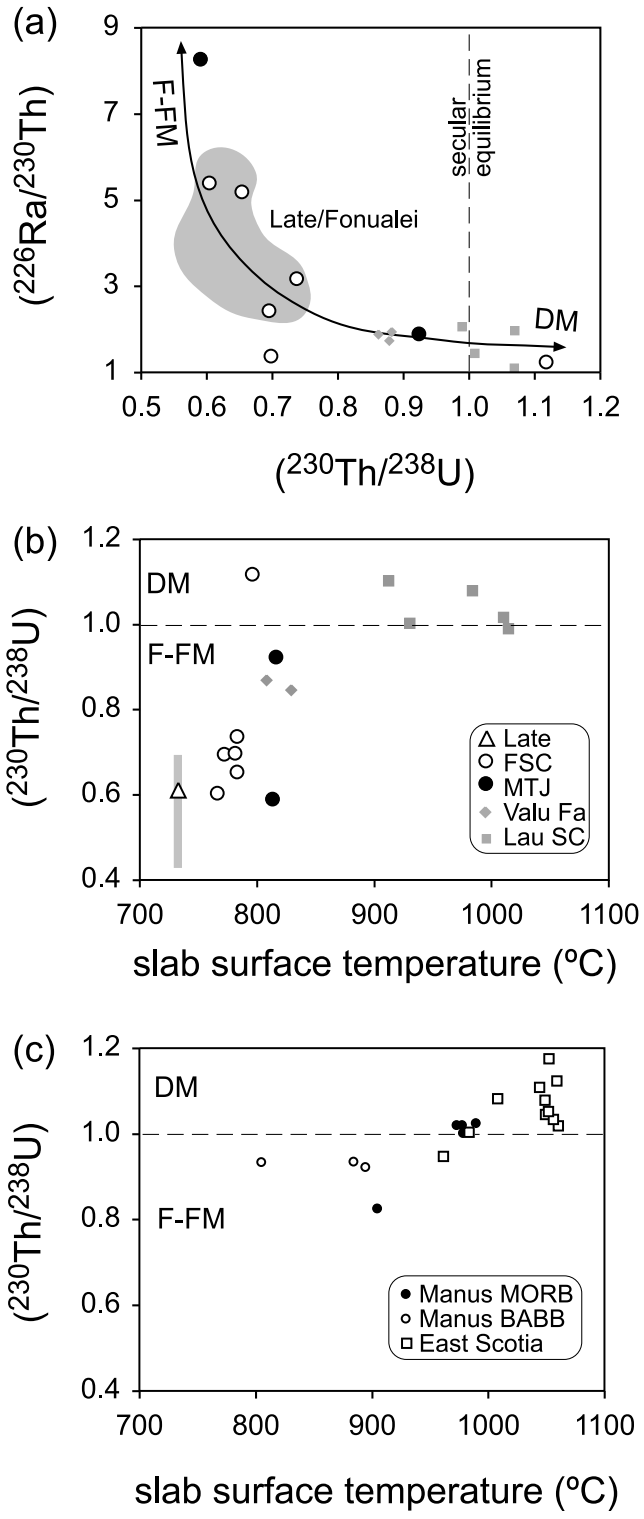

Figure 9. (a) Plot of (^{226}Ra/^{230}Th) versus (^{230}Th/^{238}U) for the Fonualei Spreading Center data and other data from the central Tonga arc [*Caulfield et al.*, 2012; *Turner et al.*, 2012]. F-FM and DM indicate the direction of displacement for fluid-fluxed and decompression melting, respectively. (b) Plot of (^{230}Th/^{238}U) versus slab surface temperature which was taken from the *Syracuse et al.* [2010] curve on Figure 5c. Plotted for comparison in Figures 9a and 9b are data from Lau Basin samples [*Peate et al.*, 2001] with MgO > 6 wt.% and slab-surface temperatures in Figure 9b calculated from their H_2O/Ce ratios using the geothermometer of *Plank et al.* [2009] and H_2O data from *Kent et al.* [2002]. (c) Plot of (^{230}Th/^{238}U) versus inferred slab surface temperature for the two other back-arc basins for which there are both U-series data and for which H_2O/Ce are available permitting estimates of slab surface temperatures (Manus Basin data from *Beier et al.* [2010]; East Scotia data from *Fretzdorff et al.* [2002, 2003]).

6. Comparison With Other Studies

[40] In contrast to *Keller et al.* [2008], who used 2-D maps to infer that Nb/Yb, Ba/Yb, Ba/La and Nb/Ta do not vary with depth to the slab along the Fonualei Spreading Center, we find that several key geochemical indices (including Ba/La) do in fact show good correlations with depth (Figures 4 and 6a). We believe that these trends arise due to a combination of two processes: (1) a decrease in the effect of slab-derived contributions and (2) an increasing contribution from plume-like components. Changes due to the first process have been observed previously from other spreading centers in the Lau Basin [e.g., *Pearce et al.*, 1995] and *Todd et al.* [2010] came to the same conclusions for cross-chain volcanism in the Havre Trough in the Kermadec arc to the south. The second process is unique to the northern end of the Fonualei Spreading Center and its location in the northeastern Lau Basin where plume mantle infiltrates the back-arc mantle wedge.

[41] ^{238}U and ^{226}Ra excesses are correlated in the Fonualei Spreading Center lavas and indicate that the primary cause of partial melting is fluid-fluxing whereas the dominance of ^{230}Th excesses in the Eastern and Central Lau Spreading

Center lavas and Niuafo'ou lavas [*Peate et al.*, 2001; *Regelous et al.*, 2008] provides evidence for a transition to decompression-dominated melting. Turning to the other two back-arc systems for which there are U-series data, *Fretzdorff et al.* [2003] found mainly ^{230}Th excesses in the East Scotia back-arc lavas although one segment is dominated by ^{238}U excess. In the Manus Basin, *Beier et al.* [2010] observed a good correlation between lavas with arc-like trace element signatures (BABB) and the presence of ^{238}U and ^{226}Ra excesses whereas MORB-like lavas had ^{230}Th excesses. Figure 9c provides evidence that, in these other two back-arc systems, a change from fluid-fluxed to decompression-dominated melting occurs when inferred slab surface temperatures are ~900–1000°C.

[42] In detail, the Manus study showed that BABB dominate lavas dredged closest to the arc whereas both BABB and MORB are found interspersed along the more distant Manus Spreading Center [*Beier et al.*, 2010]. It would appear, therefore, that there may be no *simple* pattern or gradual transition from fluid-fluxed to decompression melting in the three back-arcs, at least from the perspective of U-series disequilibria (Figures 9b and 9c). The U-series evidence provides a new perspective on, and appears consistent with, recent models based on major element systematics for contributions of both fluid-fluxed and decompression-dominated melts in the back-arc regime [e.g., *Langmuir et al.*, 2006; *Kelley et al.*, 2006; *Bézos et al.*, 2009]. However, it is not clear from Figures 8b and 8c whether this is a continuum and other influencing factors, such as changes in oxygen fugacity, that have been inferred both in the Manus Basin [*Beier et al.*, 2010] and near the Mangatolu Triple Junction [*Keller et al.*, 2008], may need to be taken into account in future work. Nevertheless, so long as it is accepted that the fluid-flux disequilibria signals (i.e., ^{238}U and ^{226}Ra excesses) originate from the slab, models of fast migration through high-porosity channels [e.g., *Turner et al.*, 2001a] must be favored over slower diapiric transport [e.g., *Hall and Kincaid*, 2001].

7. Conclusions

[43] The Fonualei Spreading Center lavas afford an excellent opportunity to appraise mantle flow, slab-surface temperatures and melting dynamics in the north Tonga arc–Lau Basin. Delineation of Samoan plume mantle is not straightforward, though all reasonable indicators suggest an overall southwest direction of mantle flow consistent with seismic anisotropy data [*Smith et al.*, 2001]. In agreement with previous studies, we infer that much of the characteristic, arc-like trace element signature in these lavas derives from addition of a wet sediment melt component augmented by fluid transfer of key elements like Ba, U, Sr and Pb. Close to the Mangatolu Triple Junction, there may additionally be an influence from Samoan plume mantle and altered redox conditions. Although the amount of sediment (melt) addition is estimated to be <1%, this contributes up to 90% of the budget of incompatible elements like La [e.g., *Turner et al.*, 1997; *Escrig et al.*, 2009; *George et al.*, 2005; *Hergt and Woodhead*, 2007; *Regelous et al.*, 2010]. Slab surface temperatures are inferred to be ~720°C beneath the arc front and increase, possibly to near 866°C, toward the back-arc although we emphasize that the absolute values should be treated with caution and require further verification. Nevertheless, it is reasonable to assume that the slab surface temperatures increase with increasing depth. Both fluid and sediment melt signatures also decrease toward the back-arc and there appears to be a progression from fluid-fluxed to decompression-dominated melting, as inferred from Ba-Yb, Na_8-Fe_8 and U-series isotope systematics, when the slab surface temperature reaches ~850–950°C. The Valu Fa Ridge and the Lau Spreading Centers, to the south and west, follow a very similar trend to the Fonualei Spreading Center lavas, as do the Manus and East Scotia back-arc basins suggesting similar processes occur in these systems as well.

[44] **Acknowledgments.** We thank the Captain, officers, technical and scientific crew of the R/V *Southern Surveyor* who took part of Cruise NoToVE to the Northeast Lau Basin in October–November 2004. Peter van Keken provided the numerical model of slab surface temperature profile as well as thoughtful discussions. We thank David Peate, Terry Plank and Jim Gill for comments that helped to improve the paper and Ian Smith and an anonymous reviewer for constructive reviews. The analytical data were obtained using instrumentation funded by DEST Systemic Infrastructure Grants, ARC LIEF, NCRIS, industry partners and Macquarie University. S.T. acknowledges the support of an Australian Research Council Professorial Fellowship (DP098865). C.G.M. and C.W.D. acknowledge support by NERC grant NE/C51902X/1. This is contribution 796 from the GEMOC Key Centre (http://www.gemoc.mq.edu.au).

References

Acland, S. (1996), Magma genesis in the northern Lau Basin, S.W. Pacific, PhD dissertation, 260 pp., Durham Univ., Durham, U. K.

Beier, C., S. Turner, J. Sinton, and J. Gill (2010), Influence of subducted components on back-arc melting dynamics in the Manus Basin, *Geochem. Geophys. Geosyst.*, *11*, Q0AC03, doi:10.1029/2010GC003037.

Bevis, M., et al. (1995), Geodetic observations of very rapid convergence and back-arc extension at the Tonga arc, *Nature*, *374*, 249–251, doi:10.1038/374249a0.

Bézos, A., S. Escrig, C. H. Langmuir, P. J. Michael, and P. D. Asimow (2009), Origins of chemical diversity of back-arc basin basalts: A segment-scale study of the Eastern Lau Spreading Center, *J. Geophys. Res.*, *114*, B06212, doi:10.1029/2008JB005924.

Birck, J. L. (1986), Precision K-Rb-Sr isotope analysis-application to Rb-Sr chronology, *Chem. Geol.*, *56*, 73–83, doi:10.1016/0009-2541(86)90111-7.

Blichert-Toft, J., C. Chauvel, and F. Albarede (1997), Separation of Hf and Lu for high-precision isotope analysis of rock samples by magnetic sector-multiple collector ICP-MS, *Contrib. Mineral. Petrol.*, *127*, 248–260, doi:10.1007/s004100050278.

Brenan, J. M., H. F. Shaw, F. J. Ryerson, and D. L. Phinney (1995), Mineral-aqueous fluid partitioning of trace elements at 900°C and 2.0 GPa: Constraints on the trace element chemistry of mantle and deep crustal fluids, *Geochim. Cosmochim. Acta*, *59*, 3331–3350, doi:10.1016/0016-7037(95)00215-L.

Castillo, P. R., P. F. Lonsdale, C. L. Moran, and J. W. Hawkins (2009), Geochemistry of mid-Cretaceous Pacific crust being subducted along the Tonga-Kermadec trench: Implications for the generation of arc lavas, *Lithos*, *112*, 87–102, doi:10.1016/j.lithos.2009.03.041.

Caulfield, J. T., S. Turner, A. Dosseto, N. J. Pearson, and C. Beier (2008), Source depletion and extent of melting in the Tongan sub-arc mantle, *Earth Planet. Sci. Lett.*, *273*, 279–288, doi:10.1016/j.epsl.2008.06.040.

Caulfield, J. T., S. P. Turner, I. E. M. Smith, L. B. Cooper, and G. A. Jenner (2012), Magma evolution in the primitive, intra-oceanic Tonga arc: Petrogenesis of basaltic andesites at Tofua volcano, Tonga, *J. Petrol.*, *53*, 1197–1230, doi:10.1093/petrology/egs013.

Charlier, B. L. A., C. Ginibre, D. Morgan, G. M. Nowell, D. G. Pearson, J. P. Davidson, and C. J. Ottley (2006), Methods for the microsampling and high-precision analysis of strontium and rubidium isotopes at single crystal scale for petrological and geochronological applications, *Chem. Geol.*, *232*, 114–133, doi:10.1016/j.chemgeo.2006.02.015.

Cheng, Q., K.-H. Park, J. D. Macdougal, A. Zindler, G. W. Lugmair, H. Staudigal, J. Hawkins, and P. Lonsdale (1987), Isotopic evidence for a hotspot origin of the Louisville Seamount Chain, in *Seamounts, Islands, and Atolls*, *Geophys. Monogr. Ser.*, vol. 43, edited by B. H. Keating et al., pp. 283–296, AGU, Washington, D. C., doi:10.1029/GM043p0283.

Cheng, H., R. L. Edwards, J. Hoff, C. D. Gallup, D. A. Richards, and Y. Asmerom (2000), The half lives of uranium-234 and thorium-230, *Chem. Geol.*, *169*, 17–33, doi:10.1016/S0009-2541(99)00157-6.

Class, C., D. M. Miller, S. L. Goldstein, and C. H. Langmuir (2000), Distinguishing melt and fluid subduction components in Umnak Volcanics, Aleutian Arc, *Geochem. Geophys. Geosyst.*, *1*(6), 1004, doi:10.1029/1999GC000010.

Cooper, L. B., D. M. Ruscitto, T. Plank, P. J. Wallace, E. M. Syracuse, and C. E. Manning (2012), Global variations in H_2O/Ce: 1. Slab surface temperatures beneath volcanic arcs, *Geochem. Geophys. Geosyst.*, *13*, Q03024, doi:10.1029/2011GC003902.

Dowall, D. P., G. M. Nowell, and D. G. Pearson (2003), Chemical preconcentration procedure for high-precision analysis of Hf-Nd-Sr isotopes in geological materials by plasma ionisation multi collector mass spectrometry (PIMMS) techniques, in *Plasma Source Mass Spectrometry*, edited by K. E. Jarvis et al., *Spec. Pub. R. Soc. Chem.*, *85*, 321–337.

Elliott, T., T. Plank, A. Zindler, W. White, and B. Bourdon (1997), Element transport from slab to volcanic front at the Mariana arc, *J. Geophys. Res.*, *102*, 14,991–15,019, doi:10.1029/97JB00788.

Escrig, S., A. Bézos, S. L. Goldstein, C. H. Langmuir, and P. J. Michael (2009), Mantle source variations beneath the Eastern Lau Spreading Center and the nature of subduction components in the Lau basin-Tonga arc system, *Geochem. Geophys. Geosyst.*, *10*, Q04014, doi:10.1029/2008GC002281.

Ewart, A., K. D. Collerson, M. Regelous, J. I. Wendt, and Y. Niu (1998), Geochemical evolution within the Tonga-Kermadec-Lau arc-back-arc systems: The role of varying mantle wedge composition in space and time, *J. Petrol.*, *39*, 331–368, doi:10.1093/petroj/39.3.331.

Falloon, T. J., L. Danyushevsky, T. J. Crawford, R. Mass, J. D. Woodhead, S. M. Eggins, S. H. Bloomer, D. J. Wrights, S. K. Zlobin, and A. R. Stacey (2007), Multiple mantle plume components involved in the petrogenesis of subduction-related lavas from the northern termination of the Tonga arc and northern Lau Basin: Evidence from the geochemistry of arc and backarc submarine volcanics, *Geochem. Geophys. Geosyst.*, *8*, Q09003, doi:10.1029/2007GC001619.

Fretzdorff, S., R. A. Livermore, C. W. Devey, P. T. Leat, and P. Stoffers (2002), Petrogenesis of the back-arc East Scotia Ridge, southern Atlantic Ocean, *J. Petrol.*, *43*, 1435–1467, doi:10.1093/petrology/43.8.1435.

Fretzdorff, S., K. M. Haase, P. T. Leat, R. A. Livermore, C. D. Garbe-Schönberg, J. Fietzke, and P. Stoffers (2003), ^{230}Th-^{238}U disequilibrium in East Scotia backarc basalts: Implications for slab contributions, *Geology*, *31*, 693–696, doi:10.1130/G19469.1.

George, R., S. Turner, C. Hawkesworth, J. Morris, C. Nye, J. Ryan, and S.-H. Zheng (2003), Melting processes and fluid and sediment transport rates along the Alaska-Aleutian arc from an integrated U-Th-Ra-Be isotope study, *J. Geophys. Res.*, *108*(B5), 2252, doi:10.1029/2002JB001916.

George, R., S. Turner, J. Morris, T. Plank, C. Hawkesworth, and J. Ryan (2005), Pressure-temperature-time paths of sediment recycling beneath the Tonga-Kermadec arc, *Earth Planet. Sci. Lett.*, *233*, 195–211, doi:10.1016/j.epsl.2005.01.020.

Gill, J. B., and R. W. Williams (1990), Th isotope and U-series studies of subduction-related volcanic rocks, *Geochim. Cosmochim. Acta*, *54*, 1427–1442, doi:10.1016/0016-7037(90)90166-I.

Griffin, W. L., N. J. Pearson, E. Belousova, S. E. Jackson, S. Y. O'Reilly, E. van Achterberg, and S. R. Shee (2000), The Hf isotope composition of cratonic mantle: LAM-MC-ICPMS analysis of zircon megacrysts in kimberlites, *Geochim. Cosmochim. Acta*, *64*, 133–147, doi:10.1016/S0016-7037(99)00343-9.

Hall, P. S., and C. Kincaid (2001), Diapiric flow at subduction zones: A recipe for rapid transport, *Science*, *292*, 2472–2475, doi:10.1126/science.1060488.

Handley, H. K., S. Turner, C. G. Macpherson, R. Gertisser, and J. P. Davidson (2011), Hf-Nd isotope and trace element constraints on subduction inputs at island arcs: Limitations of Hf anomalies as sediment input indicators, *Earth Planet. Sci. Lett.*, *304*, 212–223, doi:10.1016/j.epsl.2011.01.034.

Hauri, E. H., J. Wang, J. E. Dixon, P. L. King, C. Mandeville, and S. Newman (2002), SIMS analysis of volatiles in silicate glasses: 2. Calibration, sensitivity and comparisons with FTIR, *Chem. Geol.*, *183*, 99–114.

Hauri, E. H., G. A. Gaetani, and T. H. Green (2006), Partitioning of water during melting of the Earth's upper mantle at H_2O-undersaturated conditions, *Earth Planet. Sci. Lett.*, *248*, 715–734, doi:10.1016/j.epsl.2006.06.014.

Hawkesworth, C. J., K. Gallagher, J. M. Hergt, and F. McDermott (1993), Mantle and slab contributions in arc magmas, *Annu. Rev. Earth Planet. Sci.*, *21*, 175–204, doi:10.1146/annurev.ea.21.050193.001135.

Hergt, J. M., and C. J. Hawkesworth (1994), Pb-, Sr-, and Nd-isotopic evolution of the Lau Basin: Implications for mantle dynamics during backarc opening, *Proc. Ocean Drill. Program Sci. Results*, *135*, 505–517.

Hergt, J. M., and J. D. Woodhead (2007), A critical evaluation of recent models for Lau-Tonga arc-backarc basin evolution, *Chem. Geol.*, *245*, 9–44, doi:10.1016/j.chemgeo.2007.07.022.

Hermann, J., and D. Rubatto (2009), Accessory phase control on the trace element signature of sediment melts in subduction zones, *Chem. Geol.*, *265*, 512–526, doi:10.1016/j.chemgeo.2009.05.018.

Hermann, J., and C. Spandler (2008), Sediment melts at sub-arc depths: An experimental study, *J. Petrol.*, *49*, 717–740, doi:10.1093/petrology/egm073.

Jackson, M. J., S. R. Hart, A. A. P. Koppers, H. Staudigel, J. Konter, J. Blusztajn, J. M. D. Kurz, and J. A. Russell (2007), Evidence for the return of subducted continental crust in Samoan lavas, *Nature*, *448*, 684–687, doi:10.1038/nature06048.

Johnson, M., and T. Plank (1999), Dehydration and melting experiments constrain the fate of subducted sediments, *Geochem. Geophys. Geosyst.*, *1*(12), 1007, doi:10.1029/1999GC000014.

Keller, N. S., R. J. Arculus, J. Hermann, and S. Richards (2008), Submarine back-arc lavas with arc signature: Fonualei Spreading Center, northeast Lau Basin, Tonga, *J. Geophys. Res.*, *113*, B08S07, doi:10.1029/2007JB005451.

Kelley, K. A., T. Plank, T. L. Grove, E. M. Stolper, S. Newman, and E. Hauri (2006), Mantle melting as a function of water content beneath back-arc basins, *J. Geophys. Res.*, *111*, B09208, doi:10.1029/2005JB003732.

Kent, A. J. R., D. W. Peate, S. Newman, E. M. Stolper, and J. A. Pearce (2002), Chlorine in submarine glasses from the Lau Basin: Seawater contamination and constraints on the composition of slab-derived fluids, *Earth Planet. Sci. Lett.*, *202*, 361–377, doi:10.1016/S0012-821X(02)00786-0.

Kessel, R., M. W. Schmidt, P. Ulmer, and T. Pettke (2005), Trace element signature of subduction-zone fluids, melts and supercritical liquids at 120–180 km depth, *Nature*, *437*, 724–727, doi:10.1038/nature03971.

Klein, E. M., and C. H. Langmuir (1987), Global correlations of ocean ridge basalt chemistry with axial depth and crustal thickness, *J. Geophys. Res.*, *92*, 8089–8115, doi:10.1029/JB092iB08p08089.

Langmuir, C. H., A. Bézos, S. Escrig, and S. W. Parman (2006), Chemical systematics and hydrous melting of the mantle in back-arc basins, in *Back-Arc Spreading Systems: Geological, Biological, Chemical, and Physical Interactions*, *Geophys. Monogr. Ser.*, vol. 166, edited by D. M. Christie et al., pp. 87–146, AGU, Washington, D. C., doi:10.1029/166GM07.

Lundstrom, C. C. (2003), Uranium-series disequilibria in mid-ocean ridge basalts: Observations and models of basalt genesis, *Rev. Mineral. Petrol.*, *52*, 175–214.

Lupton, J. E., R. J. Arculus, R. R. Greene, L. J. Evans, and C. I. Goddard (2009), Helium isotope variations in seafloor basalts from the Northwest Lau Backarc Basin: Mapping the influence of the Samoan hotspot, *Geophys. Res. Lett.*, *36*, L17313, doi:10.1029/2009GL039468.

Manning, C. E. (2004), The chemistry of subduction-zone fluids, *Earth Planet. Sci. Lett.*, *223*, 1–16, doi:10.1016/j.epsl.2004.04.030.

Martin, L. A., B. J. Wood, S. Turner, and T. Rushmer (2011), Experimental measurements of trace element partitioning between lawsonite, zoisite and fluid and their implication for the composition of arc magmas, *J. Petrol.*, *52*, 1049–1075, doi:10.1093/petrology/egr018.

McKenzie, D. (1985), ^{230}Th-^{238}U disequilibrium and the melting process beneath ridge axes, *Earth Planet. Sci. Lett.*, *72*, 149–157, doi:10.1016/0012-821X(85)90001-9.

Michael, P. (1988), The concentration, behavior and storage of H_2O in the suboceanic upper mantle: Implications for mantle metasomatism, *Geochim. Cosmochim. Acta*, *52*, 555–566, doi:10.1016/0016-7037(88)90110-X.

Miller, D. M., S. L. Goldstein, and C. H. Langmuir (1994), Cerium/lead and lead isotope ratios in arc magmas and the enrichment of lead in the continents, *Nature*, *368*, 514–520, doi:10.1038/368514a0.

Newman, S., and J. B. Lowenstern (2002), VolatileCalc: A silicate melt-H_2O-CO_2 solution model written in Visual Basin for Excel, *Comput. Geosci.*, *28*, 597–604, doi:10.1016/S0098-3004(01)00081-4.

Newman, S., E. Stolper, and R. Stern (2000), H_2O and CO_2 in magmas from the Mariana arc and back arc systems, *Geochem. Geophys. Geosyst.*, *1*(5), 1013, doi:10.1029/1999GC000027.

Nichols, G. T., P. J. Wyllie, and C. R. Stern (1994), Subduction zone melting of pelagic sediments constrained by melting experiments, *Nature*, *371*, 785–788, doi:10.1038/371785a0.

Nowell, G. M., D. G. Pearson, C. J. Ottley, and J. Schweiters (2003), Long-term performance characteristics of a plasma ionisation multi-collector mass spectrometer (PIMMS): The ThermoFinnigan Neptune, in *Plasma Source Mass Spectrometry*, edited by K. E. Jarvis et al., *Spec. Pub. R. Soc. Chem.*, *85*, 307–320.

Pearce, J. A. (2005), Mantle preconditioning by melt extraction during flow: Theory and petrogenetic implications, *J. Petrol.*, *46*, 973–997, doi:10.1093/petrology/egi007.

Pearce, J. A., M. Ernewein, S. H. Bloomer, L. M. Parson, B. J. Murton, and L. E. Johnson (1995), Geochemistry of Lau Basin volcanic rocks: Influence of ridge segmentation and arc proximity, in *Volcanism Associated With Extension at Consuming Plate Margins*, edited by J. L. Smellie, *Geol. Soc. Spec. Publ.*, *81*, 53–75.

Pearce, J. A., P. D. Kempton, and J. B. Gill (2007), Hf-Nd evidence for the origin and distribution of mantle domains in the SW Pacific, *Earth Planet. Sci. Lett.*, *260*, 98–114, doi:10.1016/j.epsl.2007.05.023.

Peate, D. W., T. F. Kokfelt, C. J. Hawkesworth, P. W. van Calsteren, J. M. Hergt, and J. A. Pearce (2001), U-series isotope data on Lau Basin glasses: The role of subduction-related fluids during melt generation in back-arc basins, *J. Petrol.*, *42*, 1449–1470, doi:10.1093/petrology/42.8.1449.

Pfänder, J. A., C. Munker, A. Stracke, and K. Mezger (2007), Nb/Ta and Zr/Hf in ocean island basalts—Implications for crust-mantle differentiation and the fate of niobium, *Earth Planet. Sci. Lett.*, *254*, 158–172, doi:10.1016/j.epsl.2006.11.027.

Pin, C., and J. F. S. Zalduegui (1997), Sequential separation of light rare-earth elements, thorium and uranium by miniaturized extraction chromatography: Application to isotopic analyses of silicate rocks, *Anal. Chim. Acta*, *339*, 79–89, doi:10.1016/S0003-2670(96)00499-0.

Plank, T., and C. H. Langmuir (1998), The chemical composition of subducting sediment and its consequences for the crust and mantle, *Chem. Geol.*, *145*, 325–394, doi:10.1016/S0009-2541(97)00150-2.

Plank, T., L. B. Cooper, and C. E. Manning (2009), Emerging geothermometers for estimating slab surface temperatures, *Nat. Geosci.*, *2*, 611–615, doi:10.1038/ngeo614.

Regelous, M., K. D. Collerson, A. Ewart, and J. I. Wendt (1997), Trace element transport rates in subduction zones: Evidence from Th, Sr and Pb isotope data for Tonga-Kermadec arc lavas, *Earth Planet. Sci. Lett.*, *150*, 291–302, doi:10.1016/S0012-821X(97)00107-6.

Regelous, M., S. Turner, T. J. Falloon, P. Taylor, J. Gamble, and T. Green (2008), Mantle melting conditions during the genesis of basalts erupted at Niuafo'ou volcano, northern Lau back-arc basin, *Contrib. Mineral. Petrol.*, *156*, 103–118, doi:10.1007/s00410-007-0276-7.

Regelous, M., J. Gamble, and S. Turner (2010), Mechanism and timing of Pb transport from subducted oceanic crust and sediment to the mantle source of arc lavas, *Chem. Geol.*, *273*, 46–54, doi:10.1016/j.chemgeo.2010.02.011.

Salters, V. J. M., S. Mallick, S. R. Hart, C. H. Langmuir, and A. Stracke (2011), Domains of the depleted mantle: New evidence from hafnium and neodymium isotopes, *Geochem. Geophys. Geosyst.*, *12*, Q08001, doi:10.1029/2011GC003617.

Schmidt, M. W., and S. Poli (1998), Experimentally based water budgets for dehydrating slabs and consequences for arc magma generation, *Earth Planet. Sci. Lett.*, *163*, 361–379, doi:10.1016/S0012-821X(98)00142-3.

Sims, K. W. W., et al. (2008), An inter-laboratory assessment of the Th isotopic composition of synthetic and rock standards, *Geostand. Geoanal. Res.*, *32*, 65–91, doi:10.1111/j.1751-908X.2008.00870.x.

Smith, G. P., D. A. Wiens, K. M. Fischer, L. M. Dorman, S. C. Webb, and J. A. Hildebrand (2001), A complex pattern of mantle flow in the Lau backarc, *Science*, *292*, 713–716, doi:10.1126/science.1058763.

Spandler, C., J. Mavrogenes, and J. Hermann (2007), Experimental constraints on element mobility from subducted sediments using high-P synthetic fluid/melt inclusion, *Chem. Geol.*, *239*, 228–249, doi:10.1016/j.chemgeo.2006.10.005.

Stalder, R., S. F. Foley, G. P. Brey, and L. Horn (1998), Mineral-aqueous fluid partitioning of trace elements at 900–1200°C and 3.0–5.7 GPa: New experimental data for garnet, clinopyroxene and rutile, and implications for mantle metasomatism, *Geochim. Cosmochim. Acta*, *62*, 1781–1801, doi:10.1016/S0016-7037(98)00101-X.

Stepanov, A. S., J. Hermann, D. Rubatto, and R. P. Rapp (2012), Experimental study of monazite/melt partitioning with implications for the REE, Th and U geochemistry of crustal rocks, *Chem. Geol.*, *300–301*, 200–220, doi:10.1016/j.chemgeo.2012.01.007.

Syracuse, E. M., P. E. van Keken, and G. A. Abers (2010), The global range of subduction zone thermal models, *Phys. Earth Planet. Inter.*, *183*, 73–90, doi:10.1016/j.pepi.2010.02.004.

Taylor, B., and F. Martinez (2003), Back-arc basin basalt systematics, *Earth Planet. Sci. Lett.*, *210*, 481–497, doi:10.1016/S0012-821X(03)00167-5.

Todd, E., J. B. Gill, R. J. Wysoczanski, M. R. Handler, I. C. Wright, and J. A. Gamble (2010), Sources of constructional cross-chain volcanism in the southern Havre Trough: New insights from HFSE and REE concentration and isotope systematics, *Geochem. Geophys. Geosyst.*, *11*, Q04009, doi:10.1029/2009GC002888.

Tollstrup, D. L., and J. B. Gill (2005), Hafnium systematics of the Mariana arc: Evidence for sediment melt and residual phases, *Geology*, *33*, 737–740, doi:10.1130/G21639.1.

Turner, S., and C. Hawkesworth (1997), Constraints on flux rates and mantle dynamics beneath island arcs from Tonga-Kermadec lava geochemistry, *Nature*, *389*, 568–573, doi:10.1038/39257.

Turner, S., and C. Hawkesworth (1998), Using geochemistry to map mantle flow in the Lau Basin, *Geology*, *26*, 1019–1022, doi:10.1130/0091-7613(1998)026<1019:UGTMMF>2.3.CO;2.

Turner, S., C. Hawkesworth, N. Rogers, J. Bartlett, T. Worthington, J. Hergt, J. Pearce, and I. Smith (1997), ^{238}U-^{230}Th disequilibria, magma petrogenesis and flux rates beneath the depleted Tonga-Kermadec island arc, *Geochim. Cosmochim. Acta*, *61*, 4855–4884, doi:10.1016/S0016-7037(97)00281-0.

Turner, S., B. Bourdon, C. Hawkesworth, and P. Evans (2000), ^{226}Ra-^{230}Th evidence for multiple dehydration events, rapid melt ascent and the time scales of differentiation beneath the Tonga-Kermadec island arc, *Earth Planet. Sci. Lett.*, *179*, 581–593, doi:10.1016/S0012-821X(00)00141-2.

Turner, S., P. Evans, and C. Hawkesworth (2001a), Ultra-fast source-to-surface movement of melt at island arcs from ^{226}Ra-^{230}Th systematics, *Science*, *292*, 1363–1366, doi:10.1126/science.1059904.

Turner, S., P. van Calsteren, N. Vigier, and L. Thomas (2001b), Determination of thorium and uranium isotope ratios in low-concentration geological materials using a fixed multicollector ICP-MS, *J. Anal. At. Spectrom.*, *16*, 612–615, doi:10.1039/b008351h.

Turner, S., M. Handler, I. Bindeman, and K. Suzuki (2009), New insights into the origin of O-Hf-Os isotope signatures in arc lavas from Tonga-Kermadec, *Chem. Geol.*, *266*, 187–193, doi:10.1016/j.chemgeo.2009.05.027.

Turner, S., C. Beier, Y. Niu, and C. Cook (2011), U-Th-Ra disequilibria and the extent of off-axis volcanism across the East Pacific Rise at 9°30′N, 10°30′N and 11°20′N, *Geochem. Geophys. Geosyst.*, *12*, Q0AC12, doi:10.1029/2010GC003403.

Turner, S., J. Caulfield, T. Rushmer, M. Turner, S. Cronin, I. Smith, and H. Handley (2012), Magma evolution in the primitive, intra-oceanic Tonga arc: Rapid petrogenesis of dacites at Fonualei volcano, *J. Petrol.*, *53*, 1231–1253, doi:10.1093/petrology/egs005.

Weiss, D., B. Kieffer, C. Maerschalk, W. Pretorius, and J. Barling (2005), High-precision isotopic characterization of USGS BHVO-1 and BHVO-2 reference materials, *Geochem. Geophys. Geosyst.*, *6*, Q02002, doi:10.1029/2004GC000852.

Wendt, J. I., M. Regelous, C. Collerson, and A. Ewart (1997), Evidence for a contribution from two mantle plumes to island-arc lavas from northern Tonga, *Geology*, *25*, 611–614, doi:10.1130/0091-7613(1997)025<0611:EFACFT>2.3.CO;2.

Wiens, D. A., K. A. Kelley, and T. Plank (2006), Mantle temperature variations beneath back-arc spreading centers inferred from seismology, petrology and bathymetry, *Earth Planet. Sci. Lett.*, *248*, 30–42, doi:10.1016/j.epsl.2006.04.011.

Workman, R. K., and S. R. Hart (2005), Major and trace element composition of the depleted MORB mantle (DMM), *Earth Planet. Sci. Lett.*, *231*, 53–72, doi:10.1016/j.epsl.2004.12.005.

Workman, R. K., S. R. Hart, M. Jackson, M. Regelous, K. A. Farley, J. Blusztajn, M. Kurz, and H. Staudigel (2004), Recycled metasomatized lithosphere as the origin of the enriched mantle II (EM2) end-member: Evidence from the Samoan volcanic chain, *Geochem. Geophys. Geosyst.*, *5*, Q04008, doi:10.1029/2003GC000623.

Zellmer, K. E., and B. Taylor (2001), A three-plate kinematic model for Lau Basin opening, *Geochem. Geophys. Geosyst.*, *2*(5), 1020, doi:10.1029/2000GC000106.